Summer Internship 2016

Clean Technologies Research

Vol. 4

DE-NA0000672

PREC

PUERTO RICO ENERGY CENTER

Summer Internship 2016

August 26, 2016

Clean Technologies Research

Editors

Suheilie Rodríguez González, BS

Armando Soto Guerrero, Web Master

Sandra Pedraza Torres, MSE

Clean Technologies Research

The PREC Summer Internship began in 2010 as a tool to provide a research experience to college students, as part of the efforts of the US DoE Massie Chair of Excellence grant (DE-NA0000672) and Universidad del Turabo Puerto Rico Energy Center. This experience included working on a research project, writing a scientific paper and preparing and providing a technical presentation to their peers and receiving technical workshops that have range from literature review techniques all the way to table etiquette. For most of the participating students this was their first experience doing research and has served them to pursue careers in research in the academia, private sector and government. Their scientific work has allowed our students to further work on it and publish in peer reviews journals and proceedings. Around 40 mentors and 120 students have benefited from the program, and thru the years the quality and diversification of the participating projects have been remarkable. It is our goal to continue providing successful research experience to undergrad and graduate students as well as improve the research capabilities and research products of the Universidad del Turabo and Puerto Rico

Roberto Lorán, PhD
Principal Investigator
Samuel P. Massie Chair
Program of Excellence-DoE

Amaury Malavé, PhD
Executive Director
Puerto Rico Energy
Center (PREC)

Preface

Preface

Clean Technologies Research

2011 Summer Internship

PUERTO RICO ENERGY CENTER

Universidad del TURABO

INTECO

PROGRAM
MASSIE CHAIR OF EXCELLENCE
GRANT DE-FG02-95EW12610-A010

2012 Summer Internship

PUERTO RICO ENERGY CENTER

Universidad del TURABO

INTECO

PROGRAM
MASSIE CHAIR OF EXCELLENCE
GRANT DE-FG02-95EW12610-A010

2014 Summer Internship

PUERTO RICO ENERGY CENTER

Universidad del TURABO

INTECO

PROGRAM
MASSIE CHAIR OF EXCELLENCE
GRANT DE-FG02-95EW12610-A010

Summer Internship 2016

August 26, 2016

Clean Technologies Research

Clean Technologies Research

Contents

Contents

Biosensing System for Cancer Detection

Kemuel Torres Martinez[1], Miguel Goenaga[1], Lisandro Cunci, PhD[2]
[1]Universidad del Turabo, Puerto Rico, USA, ktorres126@email.suagm.edu[1]
[2]Universidad del Turabo, Puerto Rico, USA, cuncil1@suagm.edu

Abstract – Cancer is a life treating disease that, depending on the time of diagnosis, can change the prognosis of the patients. For this reason, accurate and fast diagnostic tools are required to be developed. Biosensors are devices that recognize a biological component and transduces their detection into readable outputs for electronic systems to understand and process. However, Biosensing Systems are expensive and require experts to operate, which are not available in many parts of the world such as Puerto Rico. In this project, we are developing a biosensor that will use the fluorescence of carbon-based nanoparticles as indication of the presence of cancer cells. Our goal is to measure the change in wavelength of the fluorescence using a Raspberry Pi V3 with an 8MP digital camera that uses a Bayer filter for color identification. Due to the importance to measure the real wavelength emitted by the nanoparticles, we focused on accessing the Bayer data directly from the image sensor array. Moreover, the fluorescence process requires a very low background light in order to be measured due to the low efficiency of this physical phenomenon; therefore, a 3D printed case was designed to comply with these requirements. Fast prototyping was allowed by the use of a CNC machine and FormLabs 1+ 3D printer. Future work will be focused on the use of the Bayer data as an array of multiple red, green, and blue sensors to identify the change in color due to the presence of cancer.

I. Introduction

The goal of this internship was to design and develop a simple prototype to be used in light color fluorescence by graphene oxide quantum dots when expose to specific wavelength. Control and process via Raspberry Pi and the Raspberry Pi Camera Board V2. Next, we will explain the steps done during this summer internship that include design and development of both the circuit and case.

II. Design and Developing Process

A. Circuit Design and Developing Process

1) Ref. [1] for the circuit design process we use the Eagle software to create the PCB circuit using commercial component sizes from the software library. This circuit was designed to be controlled from a Raspberry Pi 3, the General-purpose input/output (GPIO) pins. In this part, we worked on making two circuits:

a) RGB circuit

This circuit is composed of a transistor to work as an on/off switch, a resistance to acquire the current needed and a led RGB bulb as shown in Fig. 1.

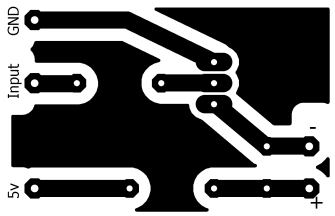

Fig. 1 RGB circuit PCB layout

b) Ultra violet circuit

This circuit is very similar to the RGB circuit in that it is composed of a transistor to work as an on/off switch, a resistance to obtain the current needed and a UV led bulb as shown in Fig. 2

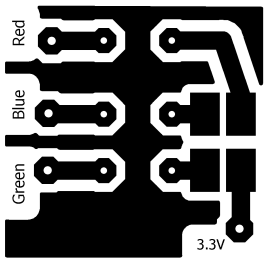

Fig. 2 UV circuit PCB layout

2) For the circuit developing process, there were two methods used, a chemical and a mechanical process of applying the PCB pattern to a copper sheet. The objective of these procedures is to make divisions between the connections we want the current to pass through and the rest of the copper material. In both of these methods, we cut the copper sheets to a smaller size using a saw machine and the borders were grinded down using a grinding machine.

a) Ferric chloride process

In this process, the $FeCl_3$ in its solid powder state was mix with H_2O to obtain a 40% concentration, Ref. [2]. Then, the solution is applied to the exposed copper sheet. The copper that is not cover with paint due to the laser etching in the desire PCB pattern will be dissolved leaving only the painted pattern. After the PCB was left for half an hour in the ferric chloride solution, the copper sheet was removed and washed with water removing the excess solution from the sheet. Finally, the paint was removed with a fine wet sand paper leaving in the copper pattern the final circuit as shown in Figure 3.

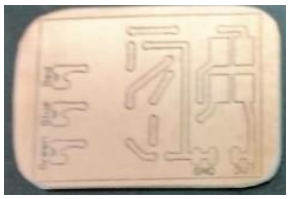
Fig. 3 Chemically etching circuit

b) Mechanical Process

In the mechanical process we used a Computer Numeric Control machine also known as CNC. This machine works by controlling 4 stepper motors, three of them for vector movement (X, Y, Z) and one for a drill. By using a drill, it removes the layer of copper from a copper sheet in the form of the circuit PCB outline. The CNC process is shown in Figure 4.


Fig. 4 CNC etching

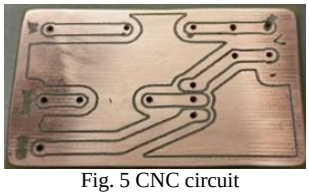
Fig. 5 CNC circuit

Using both methods we found that the CNC method was the preferred choice because it produces less waste compared to ferric chloride, and it is faster for prototyping, achieving the same results as shown in Figure 5. After all the components where solder in the copper etch circuit as seen in Figure 6 ends the circuit processing.

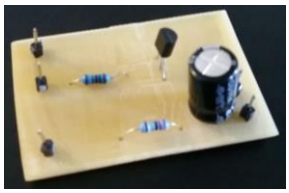
Fig. 6 Final assemble Circuit

B. Case Design and Process

1) In the case design, we used the DesignSpark Mechanical 2.0 software for 3D modeling shown in Figure 7(a), *Ref. [3]*. Using the measurement data given by the raspberry pi camera datasheet, we designed two cases to hold the camera. The first one was a small sized case while the second one was an upgraded version of the previous case design. A Form Labs 1+ resin-based 3D printer was used to obtain better resolution and higher structural strength. The end result is seen in Figure 7(b).

Case 1.0

(a) (b)

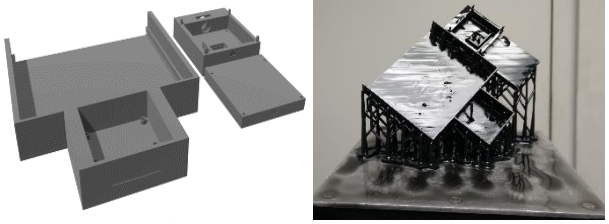
Fig. 7 Case 1.0 (a) from the 3D rendering to (b) the final printed form.


Fig. 8 Fully assemble prototype from case 1.0

The first case has three parts: a base, center and a cover. In the base, it holds the camera and a circuit board as shown in figure 8. However, after testing there was no need for the board holding area because the space used was better used as a bigger sample holding area. In the center part, there was an area to put a glass to hold the sample material. Also, this part had an groove to put color filters. The cover was a simple square shaped lid that had four guiding holes to connect to the center part. The cover worked as intended, however, the guiding pins and holes were not structurally stable. Therefore, a guiding groove was used in the upgraded version. Moreover, the upgraded version required an optimization in the distance between the camera and sample to have a better focus.

Case 2.0

(a) (b)


Fig. 9 Case 2.0 (a) from the 3D rendering to (b) the final printed form.

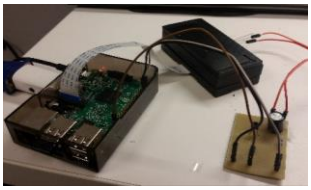
Fig. 10 Fully assemble prototype from case 2.0

In the second case designed, we improved upon the first version. We made the case bigger and also added L shape columns and grooves to connect all the parts in place to make

the case more stable, while Figure 9(a) shows the design Figure 9(b) shows the printed result. The same 3D printer as before also produced this new case designed. The final pieces can be seen in Figure 10.

III. System Testing and Controls

A. *System Testing and Controls*

For the system test, we used the circuit to illuminate polystyrene foam, and observe the details in the material, as seen in Figure 11. The focus of the camera was adjusted by rotating the camera lens. A effect we saw by adding a light color filter reduce the intensity from the source light color making the process of seeing different coloring easier as shown in Figure 12.

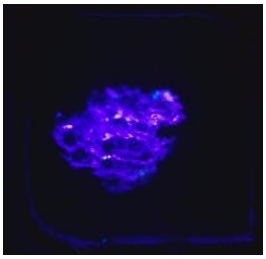

Fig. 11 UV photo no filter

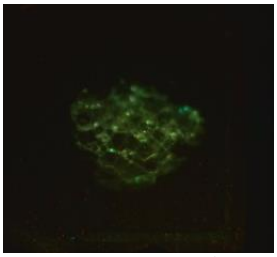

Fig. 12 UV photo filter

The camera used to take these pictures works by using a Color filter array (CFA) known as a Bayer filter, which is a matrix system known as pixels, Ref. [4]. The CFA works by allowing only light from a specific wavelength to pass through and measure each individual intensity. In the Bayer filter, each pixel has either a red, green or a blue color filter allowing that specific wavelength to pass through, as shown in Figure 13. The red, blue and green colors are the ones used because it simulates the human eye in how it detects colors. After that, the matrix values passes to a processing program that groups the pixels in areas and uses other mathematical functions to compensate and compress the matrix to a photo mostly JPEG or PNG format. Thanks to the different tests done, we found that the best way to analyze the different colors was to acquire the photo directly from the sensor data after the Bayer filter but before any processing, was done to the matrix data.

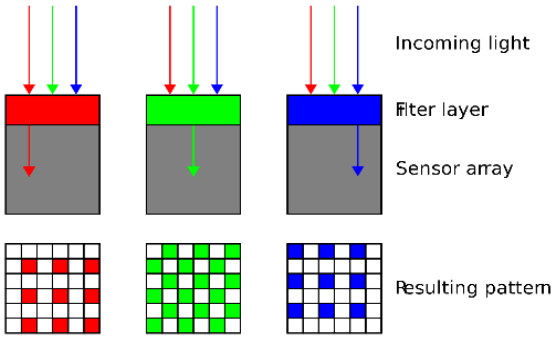

Fig. 13 Bayer Filter and matrix from http://www.astro-imaging.com/Tutorial/Narrowband_I.html

B. *For the system controls we used the Raspberry Pi*

GPIO to give power to the circuit but also control the on and off via transistor base current giving it a high (3.3v) or low (0) inputs. The camera we used to acquire photos was the Raspberry Pi Camera Board V2. By using this camera, we had access to the different integrated functions of the camera included in the device. We programed a Python based software to control the circuit and take the pictures with the desire parameters. In order to acquire the matrix RGB data directly from the camera sensor array, we used a Raw Bayer data captures program found in the camera documents, Ref. [5]. We were able to acquire the desire data and, by using the GIMP software, the photo was displayed without any modifications as shown in Figure 14 (a) with a close up in Figure 14(b). The next step is to start testing with Fluorescent Graphene Oxide Quantum Dots to upgrade the circuit, case and image processing.

(a) (b)

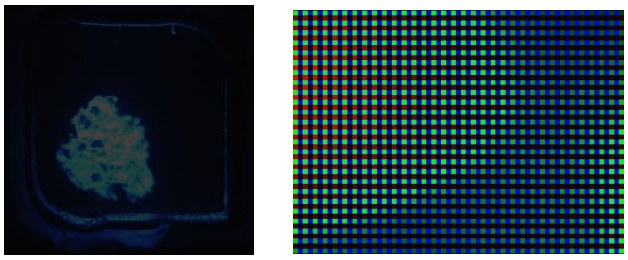

Fig. 14 Data acquired by the image sensor array shown as (a) full picture and (b) close-up to show each of the red, green, and blue sensors.

Acknowledgment

The authors of this publication acknowledge the Director of the Puerto Rico FabLab at Universidad del Turabo, Carlos I. Silva Caraballo, and the technician Rolando Carrasquillo Maldonado Turabo that guided and helped in the process of the case design and fabrication. Additionally, a recognition to all the employees at the Puerto Rico Energy Center (PREC) that helped us during this summer internship. We are very grateful for all the support given during this experience. The Puerto Rico Science, Technology and Research Trust supported research reported in this publication under agreement number 2016-00068. The content of this publication is solely the responsibility of the authors and does not necessarily represent the official views of The Puerto Rico Science, Technology and Research Trust.

References

[1] Eagle software for PCB circuit design, https://cadsoft.io/
[2] Hoskins Stephen , Pearce Roy, “The chemistry of ferric chloride”, http://www.artmondo.net/printworks/articles/ferric.htm
[3] Design Spark software for 3D product concept , http://www.rs-online.com/designspark/electronics/eng/page/mechanical
[4] Cambridge in Colour a learning community for photographers, http://www.cambridgeincolour.com/tutorials/camera-sensors.htm
[5] Raw Bayer data capture program, Picamera documentation v: release-1.9, http://picamera.readthedocs.io/en/release-1.10/recipes2.html#bayer-data

Design a program to monitor the energy from a Grid-Tie system

Pedro J. Giusti Santaella[1], Jeffrey R. Cruz Rodríguez[2], and Wilma N. Pabón -Ramírez[3], MSEE
Universidad del Turabo, Puerto Rico, USA, pgiusti1@email.suagm.edu[1], jcruz545@email.suagm.edu [2], wpabon@suagm.edu[3]

Abstract - Energy production monitoring programs are very important component in renewable energy systems. The investigation is about developing an "in house" energy monitoring system by understanding the current system and improving it. The monitoring system consists of many components including hardware and software. System operation at different weather conditions was analyzed and a new system was developed to retrieve the information directly from the meters and used in the display interface.

Keywords – energy, monitoring system

I. Introduction

Energy monitoring systems are a very popular tool in renewable energy systems. These systems monitor energy generation and consumption, and are used as historical data source and as a diagnostic tool for maintenance and improvement operations. The system consists of several components such as meters, inverters and others. There are two systems for energy generation: "Grid-Tie" system and a full generation energy system. In a grid tie system, energy is used from both in site generation and the power utility whereas in full generation all the electricity needs are full field by onsite generation systems. Depending on your setup you can have different programs for monitoring. Monitoring systems transmit data via internet to mobile devices and computers providing live data to users [1][2][3]. The particular system analysed and developed is for the Puerto Rico Energy Center (PREC) solar array system. The monitoring system consists of the renewable energy generation system, power meters, transmission equipment and display software. Electricity is generated at the array and is transmitted to the facility by a grid tie array and its characteristics (voltage, current and power) are measured at the power meter. This information is transmitted to a computer where a program reads the information and displays it in a Graphical User Interface (GUI). The current system of monitoring energy has some problems such as: delay in the readings, wrong readings, no control over the program and others. The program that is being develop will address all these problems.

A. Energy Monitoring Systems

Energy monitoring systems are systems that will show you information of energy generation and use in a facility such as a building or a house.

They are composed of three different parts: energy generator, the metering system and the user interface. The generator can be a combustion engine, solar panels, wind turbines, water turbines among others. A key component in any generation system is to measure how much energy is produced by the system as related to the energy being consumed. The energy produced which is typically electricity, is characterized by its voltage, current, frequency and phase angle. These measurements are done at the connecting point between the generation system and the facility using a power meter. The measurements are saved in a computer, where the information is displayed in a graphical user interface so that the user can see energy system performance [1][2][3]. This system is used for monitoring how much energy is being used from the generator, how much energy is being used from utility company and a combination of both. There are many systems that can be applied and they are called a *Grid-Tied* system or an *Off-Grid* System. The Grid-tied system is a combination of using electricity from electrical utility company and your own generator. The Off-Grid system is when facility has its own generating system without a connection to the utility company grid. The PREC at Universidad del Turabo (UT) is using a grid-tied system with solar panels and a wind turbine. They also have an ecological house that has its individual solar panel array. Figure 1 shows a basic energy monitoring system for a grid-tie system.

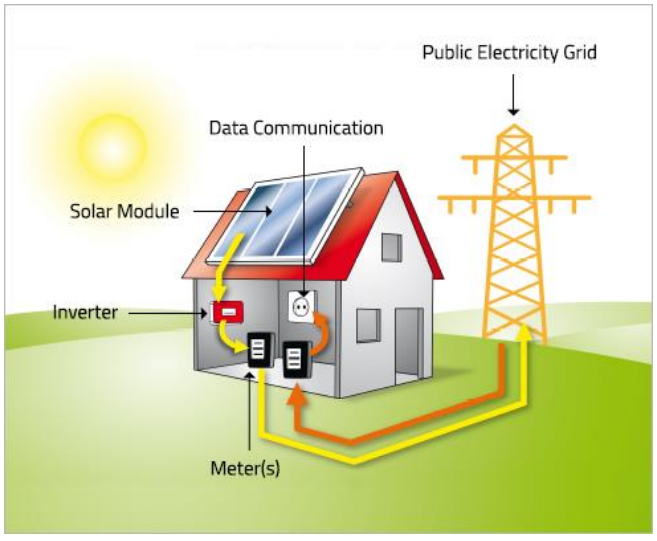

Fig. 3 Basic Grid-tie system [5]

II. Problems with the current system

The energy monitoring system that used by PREC at UT can be improved in several ways. The first improvement will be to reduce the delay in the data display. The delay is due because the data that is received from the meter [4] shown in figure 2 is not sent directly to the display program, instead the data goes to a Wi-Fi router and then goes a private server and then is received on an HTML web page where it is displayed. Figure 3 shows the HTML current system. Another area of improvement is that some of the readings that the energy monitoring system is receiving are incorrect. The monitoring system displays that the solar panels are producing a small amount of energy at night when it should not be receiving electricity. The third possible improvement is the limitation to edit or fix anything with the current program, readings or system since the software or interface cannot be modified.

Fig. 4 Shark 100 Energy Meter

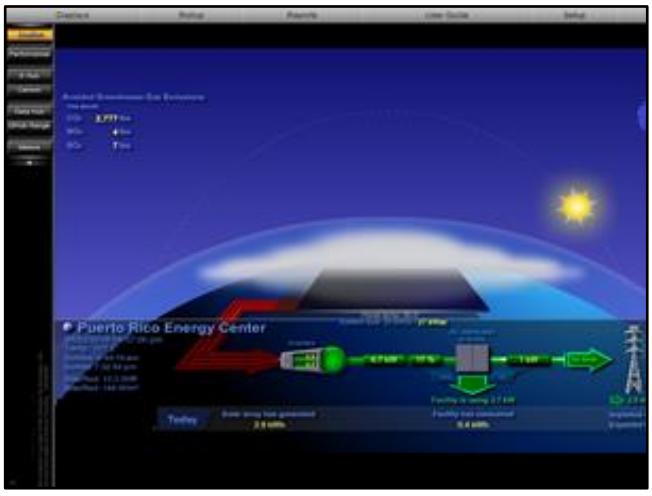

Fig. 5 Current HTML energy monitoring system used at PREC

III. Our energy monitoring system

The new system uses an "in house" developed user interface made with the programming language (PL) known as Visual Basic (VB). The reason for using VB is simplicity and familiarity of the team with the VB programming language [6]. The algorithm developed is easy to program and maintain. As a proof of concept, the team achieved to connect to the power meters and the program can reads measurements of one meter in real time successfully. The program reads any measurement from a meter, it can display the real measurements and it can be change if any error occurs.

An initial propose for an *in-house* program was developed and it features a Graphical User Interface (GUI) that displays how much energy the facility is receiving from the solar panel array and from the energy supplier; also, it displays how much of the energy is being consumed as shown in the figure 4 for PREC.

The program has a second window where it displays the same measurements parameters for the ecological house as shown in figure 5. The third window displays how much energy is being generated from the wind turbine as shown on figure 7. This window is not functional yet because there are some physical components that are not in the current system to measure that energy. The fourth window shown in figure 6 is a summary of all the other windows and readings. It will show the energy measurements from the solar panels, the energy provider on the PREC and the ecological house. In addition, there will be a bar plot showing the energy consumption and generation from the PREC and ecological house.

A. Internship Experience

We had some difficulties on the communication with the power meters at the beginning of the summer internship. The communication problem held us back for a good few weeks. The new problem emerged quickly after achieving communication [7]; the problem was that the power meters use a protocol called Modbus [8]. This protocol uses programming to access some pieces of information from a device, such as the name and such. We used a Modbus program simulator to conduct a proof of concept. As future work, we will integrate the protocol to our monitoring energy system program.

IV. Future Work

As part of the PREC summer internship, we accomplished to communicate with the power meters and start the development of the *in-house* monitoring energy system for PREC at UT. As future work, the program will read data from the four power meters at PREC and ecological house and display its measurements in the user interface. Another improvement will be to have the energy generated by the wind turbine monitored as part of the energy system developed. In addition, the program will be available via the Internet and not just on a Local Area Network (LAN). Another goal is to have the display

as aesthetically as the software being used. The final future goal is the development of an IOS and Android mobile application for the new proposed monitoring energy system, this will include programming it in other languages such as but not limited to: Java and C#.

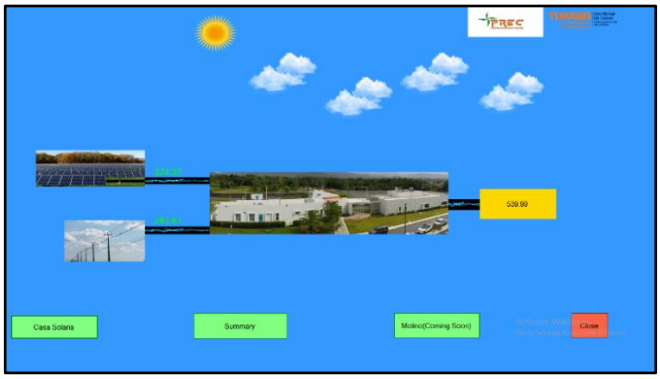

Fig. 6 Form 1 (PREC readings)

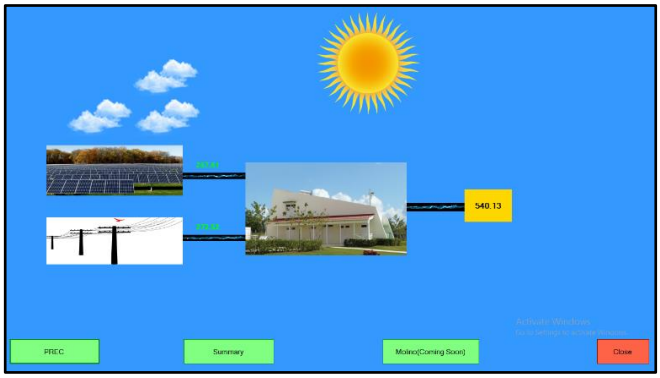

Fig. 7 Form 2 (Readings from ecological house at PREC)

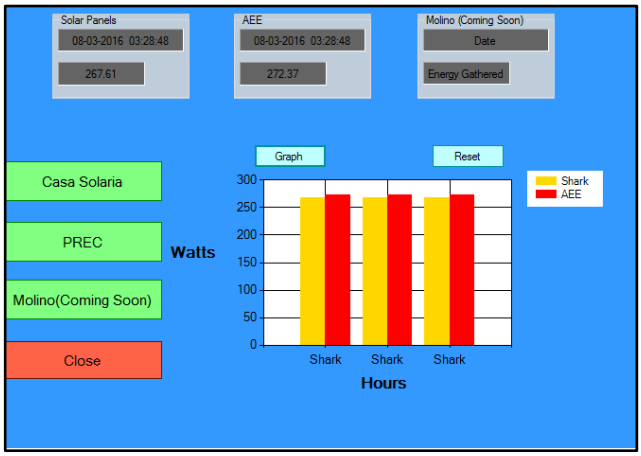

Fig. 8 Form 3 (Summary readings)

Fig. 9 Form 4 (Wind turbine readings – future work)

ACKNOWLEDGMENTS

We are fully grateful to Puerto Rico Energy Center and Massie Chair for Excellence Program Grant #DE-NA000672 at the Universidad del Turabo for this opportunity and for the funding provided for this project. We would like to recognize the collaboration, support and guidance of the engineer Ian Gutiérrez, Dr. Amaury Malavé, Sandra Pedraza, PREC staff, and our mentor Wilma N. Pabón in the improvement of our investigation.

REFERENCES

[1] A. Chouder, et. al., "Monitoring, modelling and simulation of PV systems using LabVIEW" . *Sol.Energy*. Sep. 2012.

[2] R. Nagalakshmi, et. al., "Design and development of a remote monitoring and maintenance of solar plant supervisory system", *IJECS*, vol. 3, no. 12, pp. 9382 – 9385, Dec 2014.

[3] M. Afonso, P. Pereira, & J. Martins, "Weather Monitoring System for Renewable Energy Power Production Correlation". In *Doctoral Conference on Computing, Electrical and Industrial Systems*, pp. 481-490, Feb 2011.

[4] Electro Industries/GaugeTech. (2013, March 20). *Shark 100 Multifunction Power and Energy Meters/Transducers Installation & Operation Manual* [Online]. Available: http://www.electroind.com/pdf/11_13_12_pdf/E145701_shark%2050_100_100B_Manual.pdf

[5] Energy Market Authority Singapore Government Available: www.ema.gov.sg/Solar_Photovoltaic_Systems.aspx

[6] T. Gaddis and K.R. Irvine, *Starting out with Visual Basic*, 7th Ed., Pearson, 2016.

[7] C. Severance, et.al., *Introduction to Networking: How the Internet Works*, 1st Ed., CreateSpace Independent Publishing Platform, 2015.

[8] Modbus Organization.
Available: http://www.modbus.org/

Naturopathic Approach towards Cardiovascular Diseases in Naturopathic Medicine Clinic at School of Health Sciences, Universidad del Turabo, P.R.

Lichel Báez[1], John González[1], Frank Valentín, MD[2]
[1]Universidad del Turabo, Gurabo, Puerto Rico, USA
[2]Universidad del Turabo, Gurabo, Puerto Rico, USA

Abstract- Naturopathic Medicine (NM) is a complementary form of health care, focusing on the prevention, treatment and encouragement of inheriting self-responsibility towards a patient's health. Some cardiovascular diseases can be prevented and even stopped with modifications in physical exercise and nutrition. NM is a source of clean technologies for our environment (nature). This complementary medicine brings different ways to treat diseases. This research focuses on the use of naturopathic modalities that serve as clean technologies (cleaner therapeutic interventions with less side effect or impurities) for treatment for cardiovascular diseases such as high blood pressure (hypertension) in Puerto Rico. For this study, we did a new retrospective investigation of three hundred forty-five patients (345) out of 733 in the Naturopathic Medicine Clinic of University of Turabo in its new facilities in Navarro to document demographic patient data and naturopathic approaches to cardiovascular diseases.

Keywords—Crataegus oxyacantha, Cardiovascular disease, Naturopathic Medicine, Hawthorn, Hypertension

I. Introduction

Cardiovascular Diseases (CVD) include numerous heart and vascular diseases, which ultimately relate to atherosclerosis as a pathologic mechanism of action. This condition develops when plaque builds up in the walls of our arteries. In return, it complicates blood flow which leads to blood clot. [1] Disturbance in the redox states of cells can have a toxic effect through the production of peroxides and free radicals. These form due to normal bodily processes and environmental contamination. These cause oxidative stress, which tends to build base damage, as well as DNA strain breaks. To be able to counter this, your body must produce enough anti-oxidants to neutralize the free radicals. [1]

A. Naturopathic Medicine

Naturopathic medicine is a distinct system of health care and practice of preventing, diagnosing and treating conditions of the human mind and body. [2] These consist in natural herb products unlike pharmaceuticals products and with less secondary effects. We present the principles of naturopathic medicine, in the following *Table 1*. But how does the treatment of a patient relate to clean technologies and the environment? NM promotes the healing power of nature, in other terms; it promotes the environment around the patient to contribute significantly to the healing process of diseases both physically and mentally. Cardiovascular diseases have a proven record to correlate with nutritional deficiencies. [3] Patients, which suffer from cardiovascular diseases, have many times problems with diet and exercise. Eating the right foods sometimes is not enough to promote a healthy cardiac metabolism.

Many times with need to boost our cardiovascular system with exercise and supplements, that promotes the anti-oxidation process.

TABLE 1. Principles of Naturopathic Treatment

Principles of a Naturopathic Treatment
1. The healing power of nature
2. Identity and causes
3. Do no harm
4. Doctor as a teacher
5. Treat the whole person
6. Prevention
7. Wellness

*American Association of Naturopathic Physician (AANP) [10]

II. Results

The Institution Review Board of the SUAGM (Sistema Universitario Ana G. Méndez) evaluated this study and its IRB number is 03-646-15, Undergraduate students and mentor certified in IRB, RCR, HIPSS among others to conduct this study in protection of human rights. A case-by-case clinical review was made in accordance to IRB guidance and information dissemination is in compliance with the Good Clinical Practice Guidelines (GCP).

The Naturopathic Medicine Doctoral Program Clinic (NMDP Clinic; NMC: Naturopathic Medicine Clinic) has received 733 patients since day 1 in May 2012, out of which we needed to evaluate 252 to have an acceptable rate of 5% of error and a 95% of confidence interval, with an estimated percentage level of 46% for patients with cardiovascular diseases. Inclusion criteria were broad: Mainly any patient with two blood pressure readings above 120/80 in two offices separate office visits and/or a forma diagnosis of cardiovascular disease or metabolic disease such as, but not limited to hyperlipidemia, hypercholesterolemia, diabetes mellitus, and obesity. In relation to age range, the initial cutoff was 10 y/o to 100 y/o. Therefore, the exclusion criteria were patients that did not have a formal cardiovascular disease diagnosis and had only one BP measurement above 120/80. [4] Patients personal contact information was blind using random codes, but individualized. All patients had a traditional primary care

physician at their care, which had contact with the naturopathic medicine doctor to coordinate care.

A. Age and Gender

Male and female patients of the NMDP Clinic who had cardiovascular diseases were 59 females and 57 males for a total of 116 who had a type of cardiovascular diseases (hypertension) as shown on *Table 2*. Age range was from 11 to 81 years following inclusion and exclusion criteria. Stratification was as follows: 0-24, 25-49, 50-74 and 75-100 years old.

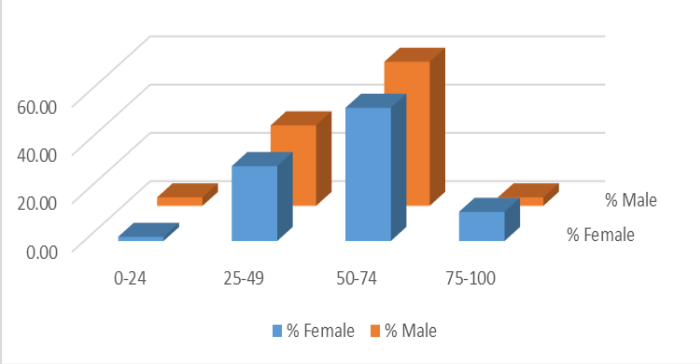

Fig. 1 Comparison by age of the patients in PNMC

B. General Common Complaint and NM Treatments in Patients

When looking at the chief complaints, we can see that 26 patients came in due to cardiovascular signs and symptoms, 19 diabetics being the second leading, and 15 patients with obesity seen in *Table 3*. When we look at combined complications such as diabetes with hypertension, diabetes with obesity or obesity with hypertension, we can see how it decreases with the latter being only of one patient.

They were almost the same amount of patients that came in with hypercholesterolemia and hyperlipidemia (5:4); in addition, there was the same amount of patients with hyperlipidemia & diabetes than patients with hypercholesterolemia, hypertension & obesity and hypercholesterolemia & hyperglycemia combined, but all were different patients and no repetition of patients were made due to blindness of study. Finally, there were two patients that came in with intermittent claudication with varicose veins and only one with circulatory problems.

The most common treatment for cardiovascular diseases at NMC at Universidad del Turabo, P.R. are listed below:

As a result, the most selected treatment modalities were: Acupuncture (was the most prescribed for patients) following, diet, vitamin D, fish oil, omega 3 are the second highest. The lowest were Melatonin, Glutamine, Milk Thistle, Tui Na Massage, Calcium, Mg, B12, Chromium piconilate and Bromelain as shown on *Fig 2*. All these helped to have a better cardiovascular system.

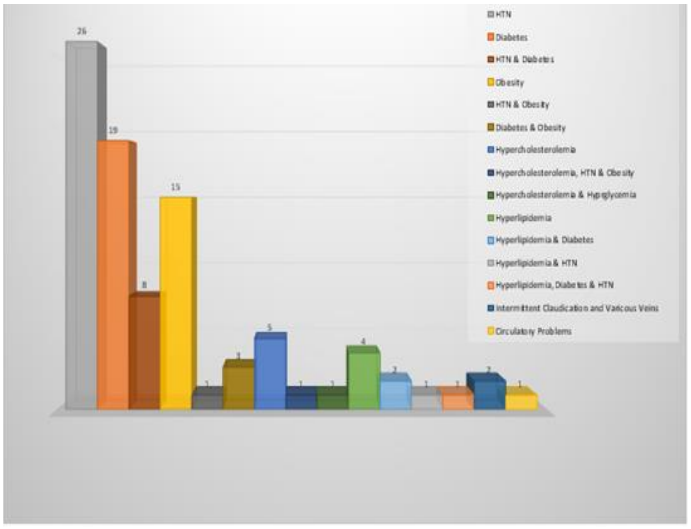

Fig. 2 Most Common Chief Complaints Related to Cardiovascular Diseases at Naturopathic Clinic of UT (Gurabo)

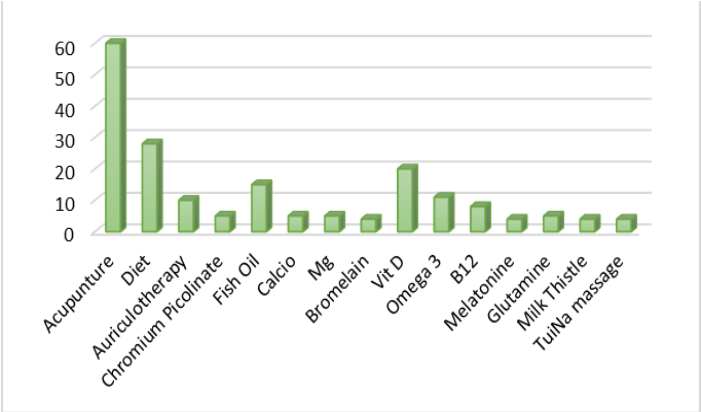

Fig 3 Most Common Treatment Modalities for Cardio Vascular Disease at Naturopathic Medicine at Navarro, PR

III. DISCUSSION AND CONCLUSION

This research is an epidemiological descriptive semi-quantitative protocol; in which we describe the population demographic at the NMDP Clinic at the new facilities in the School of Health Sciences. This step is the foundational step in order to study the natural tendencies of the cardiovascular disease population.

We conducted 345 clinical case reviews and stratified them by gender and age out of a population of 733 patients in total since the clinic formally began operation in 2008, for of 5% of error and a 95% of confidence interval, in this stratification only.

From those 345 clinical cases, only 116 patients were diagnosed with cardiovascular disease. These were stratified in the following numbers: 26 were diagnosed with Hypertension, 19 with Diabetes only, 8 with dual diagnosis such as Hypertension and Diabetes, 15 with Obesity, 2 with Hypertension and Obesity, 3 with Hypertension and Obesity, 5 with Hypercholesterolemia, Hypertension and Obesity, 1 with Hypercholesterolemia, Hypertension and Obesity. Also 1 with Hypercholesterolemia and Hyperglycemia, 4 with hyperlipidemia and hypertension, 2

with hyperlipidemia and diabetes, 1 with hyperlipidemia and diabetes and hypertension, 2 with intermittent claudication and varicose veins and 1 other with circulatory problems.

From the 116 cases more females than males are afflicted with cardiovascular disease 59 (F) to 57 (M) for 116 patients, which responds to the overall tendency that more females than males are afflicted by cardiovascular diseases. The reasons for this change are still under current investigation.

In this retrospective study the most common naturopathic modalities were also studied, from the results: Acupuncture (was the most prescribed for patients) following, Diet, Vitamin D, Fish Oil, Omega 3 are the second highest. The lowest were Melatonin, Glutamine, Milk Thistle, TuiNa massage, Calcium, Mg, B12, Chromium piconilate and Bromelain. All these helped to have a better cardiovascular system as documented in patient notes in the clinical files.

The human body is a full environment of chemical and physical reactions that work in harmony in order to maintain homeostasis. The immediate surrounding environment directly affects it, we apply external forces through traditional pharmacology to enhance and help the physiological system to obtain balance. Therefore, an adequate homeostasis will ensure an adequate use of energy.

Energy in this environment is quantified in a multiplicity of indicators such as diet (caloric intake and outtake), exercise and health. Although we take general indicators to indicate a normal health state such as mood or physiological states such as fever (infectious cases). We can agree that energy states in health are used more efficiently.

Disease therefore cause imbalance in energy states, which are detrimental to health, which therefore causes signs and symptoms of illness.

Naturopathic Medicine has a unique focus in which is contributes to treat the identified cause of the disease and improve the overall health of the patient. Therefore, in cardiovascular diseases the treatment modalities used such as acupuncture, supplement therapy, improve the energy balance of the patient. A well balanced diet will always give the adequate support of nutrients and therefore anti-oxidants, which are fundamental for the treatment of cardiovascular diseases. Supplementation improved the abundance of anti-oxidants in order to absorbed free radicals, which cause damage to cells, and cell membranes in cardiac tissues.

In the repertoire of supplements is Crataegus Oxyacantha (CO) which has a high concentration of flavonoids which are considered primarily antioxidants, for the treatment of cardiovascular diseases. [5] Although we only have one full documented patient in which CO was used, it was under specific medical conditions, in which the correct dose and the certainty of herbal drug interactions that this patient benefited from this treatment. Therefore, more investigation is needed to quantify the specific measures in which CO can be used.

ACKNOWLEDGMENT

We gratefully acknowledge the financial support and the opportunity of the Puerto Rico Energy Center (PREC) at University of Turabo, Gurabo, Puerto Rico. The academic support to this research: Dr. Nydia Bou, Dean of School of Health Sciences; Dr. Nilda I. Boria, Associated Dean of School of Health Sciences and Dr. Diannie I. Rivera, Associated Dean of School of Health Sciences. The laboratory support: Maritza Rodríguez, sciences laboratory technician.

AUTHORIZATION AND DISCLAIMER

Authors authorize PREC to publish the paper in the conference proceedings. Neither PREC nor the editors are responsible either for the content or for the implications of what is expressed in the paper.

REFERENCES

[1] American Heart Association. *What is cardiovascular disease?* Retrieved from: http://www.heart.org/HEARTORG/Caregiver/Resources/WhatisCardiovascularDisease/What-is-Cardiovascular-

[2] American Association of Naturopathic Physician. (n.d.). *House ofDelegates Position Paper Definition of Naturopathic Medicine* Retrieved from: http://www.naturopathic.org/files/Committees/HOD/Position PaperDocs/Definition Naturopathic Medicine.pdf

[3] Llanio Navarro, R., & Perdomo Gonzalez, G. (n.d.). *Propedéutica clínica y semiología médica*. Retrieved from: http://www.sld.cu/galerias/pdf/sitios/pdguanabo/cap10.pdf

[4] Organización Mundial de la Salud. Enfermedades cardiovasculares Retrieved from http://www.who.int/mediacentre/factsheets/fs317/es/

[5] Worden, J. (2014). *Netdoctor. Antioxidants and oxidative stress.* Retrieved from:http://www.netdoctor.co.uk/healthy-eating/a10835/antioxidants-and-oxidative-stress/

Thermal Effects on Li-ion Batteries due to Temperature Changes

Angel L. Mangual Rotger[1], Eimylin Achang Lopez[2], and Diego A. Aponte-Roa, MScEE[3]
[1]Universidad del Turabo, Gurabo, PR, USA, amangual7@email.suagm.edu, [3]aponted1@email.suagm.edu
[2]Universidad del Turabo, Gurabo, PR, USA eachang1@email.suagm.edu

***Abstract*– This paper presents the thermal effects on a rechargeable Li-ion battery with a voltage of 3.7V versus two CR2 Li-ion batteries models of 3V, exposed to different temperatures. Different situations were created in different environment to compare with the manufacturer's data. Result of this research gives a scientific evidence of thermal effect due to different temperatures that are present on cities and could affect the behavior of batteries typically used as power source in commercial products.**

Keywords—Li-ion Batteries, Temperature Effect, environment, Heat Stroke.

I. INTRODUCTION

Since 1990 through 2015 had been registered 754 deaths by heat stroke in the United States. In 2015 were registered 25 of them and in this year until July, there have been 11. These deaths are the second highest number of children under 14 years after back over accidents where the amount is 1282 (see figure 1) [1]. This information underestimates the magnitude of fatal accidents do not happen in a moving car. Temperatures in vehicles can rise to fatal levels between 7 to 10 minutes, although the outdoor temperature is at about 26.7 degrees Celsius [2]. Since 2012 the National Highway Traffic Safety Administration (NHTSA) produced a campaign to alert parents about the high temperatures and to avoid these tragic accidents, yet these happen.

U.S. National Non-Traffic Child Fatalities from the KidsAndCars.org Database

FATALITIES	<1989*	1990	1991	1992	1993	1994	1995	1996	1997	1998	1999	2000	2001	2002	2003	2004	2005	2006	2007	2008	2009	2010	2011	2012	2013	2014	2015	TOTAL
Backovers	25	0	3	4	5	12	10	7	11	17	24	28	53	70	106	84	108	82	102	76	86	65	78	70	60	71	50	1307
Heatstroke	20	5	5	4	11	9	24	11	21	39	32	35	39	31	43	39	47	29	36	43	33	49	33	35	44	32	25	774
Frontovers	5	0	0	1	0	0	3	0	4	5	9	7	7	8	10	27	46	67	56	66	71	76	56	49	60	64	64	761
Vehicle in Motion	13	0	1	0	1	2	0	9	1	9	9	12	10	14	18	19	17	13	22	7	11	10	11	12	14	5	6	246
Underage Driver	0	0	0	1	0	1	1	0	2	1	4	6	7	0	2	8	5	17	14	13	34	22	14	24	10	17	10	213
Power Window	20	0	0	3	1	1	1	1	5	5	2	2	3	4	5	9	3	3	1	3	2	1	1	2	1	2	0	81
Falls	0	0	0	0	0	0	0	1	0	1	1	1	2	2	2	1	3	4	0	2	11	6	5	4	7	1	1	55
Fire	2	0	0	0	1	0	0	3	0	3	2	3	3	3	4	0	3	2	6	0	2	1	3	2	0	0	4	47
Drowning	0	0	0	0	0	0	0	0	2	0	0	0	0	0	0	1	1	0	2	3	10	4	5	3	2	3	3	39
Carbon Monoxide	4	0	0	0	0	0	0	0	3	0	1	1	2	1	5	0	7	3	0	0	5	0	0	0	1	0	1	34
Left, Found Gun	0	0	0	0	1	0	0	0	0	0	0	1	0	0	1	1	0	0	1	1	0	1	1	3	0	0	1	12
Seat Belt Strangulation	1	0	0	0	0	0	1	0	1	1	0	0	3	1	1	0	2	0	0	0	0	0	0	0	0	0	0	11
Hypothermia	0	0	0	0	0	0	0	0	0	0	0	1	1	0	0	0	0	1	0	0	1	0	0	0	0	0	0	4
Backover or Frontover? (Direction unknown)	2	0	0	0	0	0	0	0	0	0	0	0	1	0	2	2	2	3	1	2	5	0	0	0	2	2	0	24
Other	3	0	0	1	0	0	0	0	0	2	0	2	1	0	2	4	4	6	6	4	6	2	2	2	0	1	1	49
YEAR TOTALS	90	5	9	13	20	25	40	32	50	81	84	97	130	134	197	189	242	221	240	214	266	235	207	204	199	195	165	3584

Data Source: KidsAndCars.org Database (as of January, 2016)
*Fatalities with unknown dates are included in the "<1989" column above.

Fig. 10 Data of the Non- Traffic Child Fatalities [1]

Recently due to the number of heat stroke death and the use of technology, it has begun work on a project to prevent these kind of tragedies. Momentum Creative Labs (MCL), Start-up company established in Puerto Rico, created Gardien Alert System for the main purpose of alerting parent when a child has been left in a car. Some of the advantages of this product is its minimal installation, small size and high reliability. The system consists of a sensor that is placed between the child and the car seat, which will send a wireless *"Bluetooth"* signal to three different modules: a keychain, a remote alarm and a smartphone, which will send an alarm when leaving the car and the baby seated in the car seat. The power source are batteries and the system could be exposes to different temperatures

To measure Gardien's battery performance, we perform an analysis of two kinds of lithium batteries: CR2 and rechargeable. To make a comparison of the battery reliability, we use two different brands: Duracell and T-energy, which are commonly use as power source in equipment such as photographic cameras, among others (see Figure 3). Two of the same model of rechargeable batteries were used to validate the result (see Figure 3). To describe the behavior at extreme temperatures and thermal shock, the measure of battery discharge according to temperature changes were perform by exposing the batteries to datasheet temperatures limits.

This project will present the discharge ratio of two different types of batteries to some variants temperatures. The research focus is to demonstrate the service life and the voltage of the batteries by proving them at extreme and drastic changes in temperature. This paper presents the battery test results.

Fig. 11 CR2 Batteries

Fig. 12 Rechargeable Battery

II. METHOD

A. Methodology of the Experiment

An experimental set-up for the verification of the effects of heating and cooling was implemented in various types of batteries. Three set of two rechargeable batteries of 3.7V and six set of two CR2 batteries models of 3V were put into a heating chamber and refrigerators. The heating chamber was implemented using a universal temperature controller (Programmable Digital Adjustor PID) F/C SSR Thermostat Temperature Controller Control Output, powered by 90-265V AC/DC, Consumption of 5VA and accuracy of 0.2%, as shown in Figure 4. The system have auto-tuning PID / Fuzzy PID Control, 7 Different Dual Output Combinations, Individually Programmable PID Control Parameters, apply with Step Control, Dual Display for Fahrenheit (F) and Celsius (C) (temperature controller TA6 SNR) [3].

Fig. 13 Ovens and PID system

PLA material was used to perform the boxes used during the experiments (see Figure 5).

Fig. 14 Set of PLA Batteries Cases

PLA filament is a newer polymer used for 3D printing (see figure 6) [5]. It is more environmentally friendly, as it is often derived from corn, even though it biodegrades slowly and not very easily even with these drawbacks. PLA is favored in enclosed areas, such as your home, and around children or those with sensitive respiratory systems as the PLA Printing Filament generates less noxious fumes.

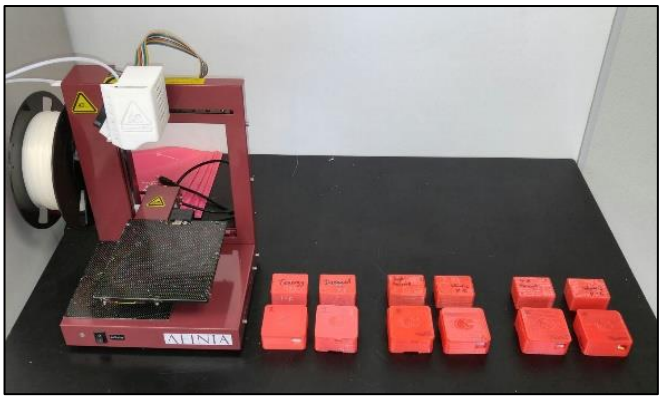

Fig. 15 Afinia 3d Printer and set of tests cases

B. Experimental Method

In test 1, were used two rechargeable batteries of 3.7V on a board with a load resistance of 280Ω and two batteries CR2 of 3V with a load resistance of 1kΩ. The battery was exposed at the upper level limit of 50ºC for a period of 96 hours in the oven (figure 4). Voltage was recorded after.

In test 2, were used two rechargeable batteries of 3.7V on a board with a load resistance of 280Ω and two batteries CR2 of 3V with a load resistance of 1kΩ. The battery was exposed at the lower level limit of -20ºC for a period of 96 hours in a refrigerator and record the voltage after.

In test 3, were used two rechargeable batteries of 3.7V on a board with a load resistance of 1kΩ and two batteries CR2 of 3V with a load resistance 3.3kΩ. Temperature was varies slightly from ambient temperature to a lower temperature. The lower temperature should base of a specific region (room temperature of 25ºC). The system was set to a constant ambient temperature of around 35ºC. Then, for a period of 4 hours a day, the battery was exposed to 40ºC inside the oven.

In test 4, were used two rechargeable batteries of 3.7V on a board with a load resistance of 1kΩ and two batteries CR2 of 3V with a load resistance of 3.3kΩ. Varies the temperature aggressively from ambient temperature to a lower temperature. The lower temperature varies from 25 to 0 Celsius degrees. Then, the sample move to a constant ambient temperature. Then, for a period of 4 hours the battery was exposed to 0 degrees inside the fridge.

C. Test Development

In order to compare the batteries' behavior, different plots were created by measuring the battery voltage. The unit used in time was days and two values were taken (am and pm). Figure 7 shows the comparison of behavior between CR2 Duracell and CR2 Tenergy after 96 hours of 50ºC limit temperature (test 1). Figure 8 shows the behavior of two rechargeable batteries at same environment.

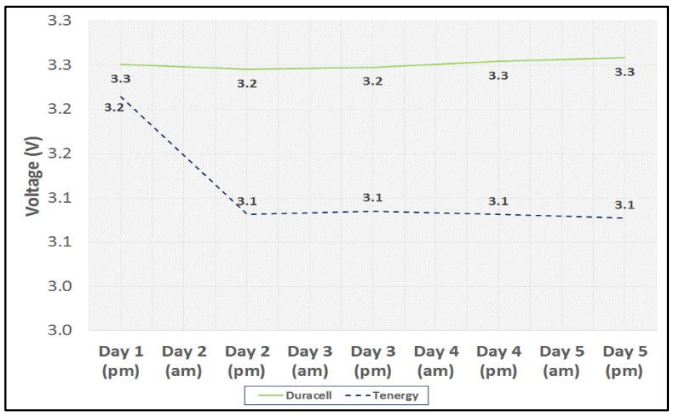

Fig. 16 Test 1 CR2: Voltage vs Time (days)

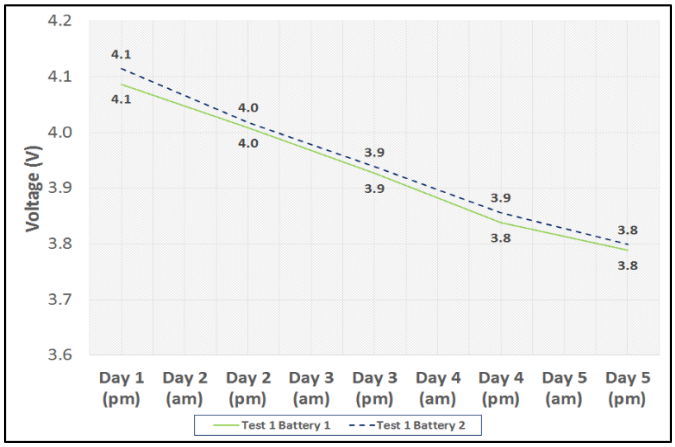

Fig. 17 Test 1 Rechargeable: Voltage vs Time (days)

Figure 9 and Figure 10 shows the batteries' behavior at -20ºC for a period of 96 hours (5 days). Figure 9 shows the CR2 batteries: Duracell and Tenergy, while Figure 10 the two rechargeable samples.

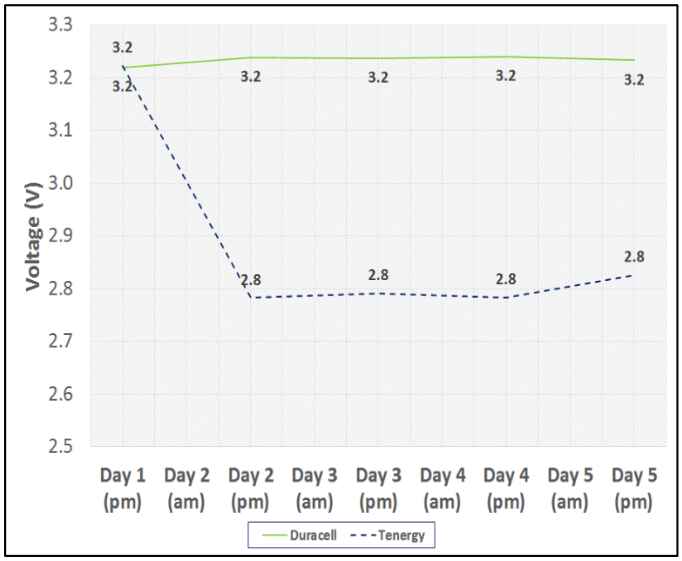

Fig. 18 Test 2 CR2 Voltage vs Time (days)

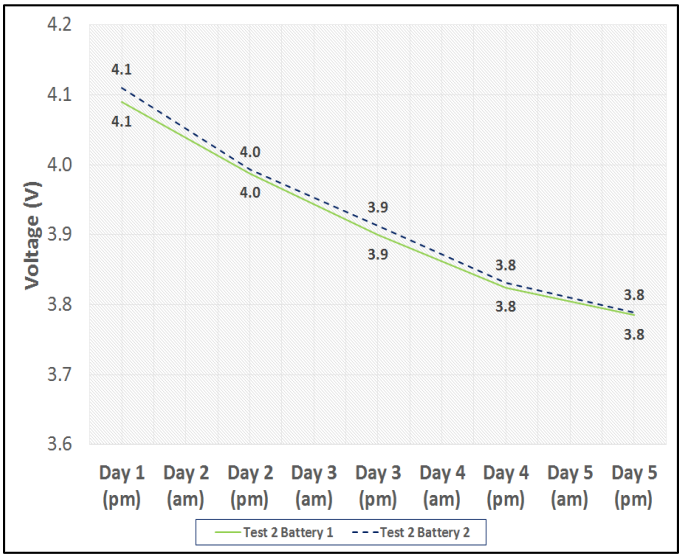

Fig. 19 Tests 2 Rechargeable Voltage vs Time (days)

Results of the battery discharge are presented in the next three figures but at different environment. Figure 11 and Figure 12 shows the discharge at 30ºC for 4 hours by a period of 28 days. Figure 11 presents the comparison of the CR2 batteries: Duracell and Tenergy. Duracell do not demonstrate any significant change while Tenergy shows a clear discharge after 19 days. Figure 12 shows how the rechargeable batteries discharge through the 28 days starting at 4.11V and finishing at 3.67V.

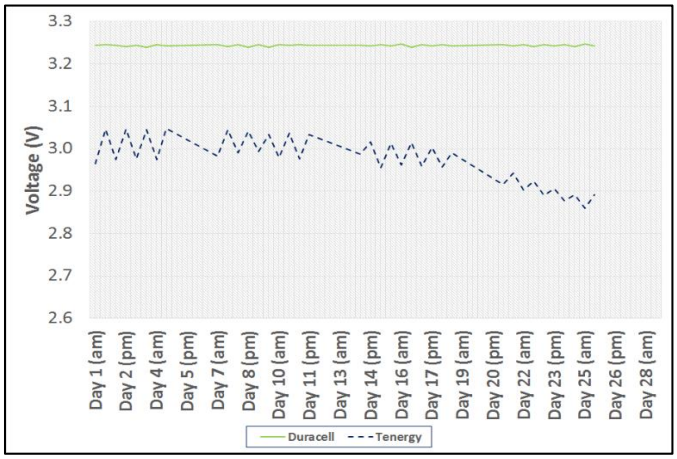

Fig. 20 Test 3 CR2 Voltage vs Time (days)

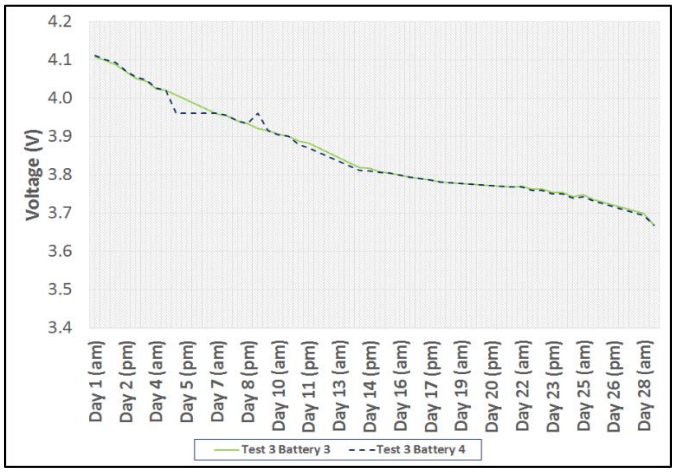

Fig. 21 Test 3 Rechargeable Voltage vs Time (days)

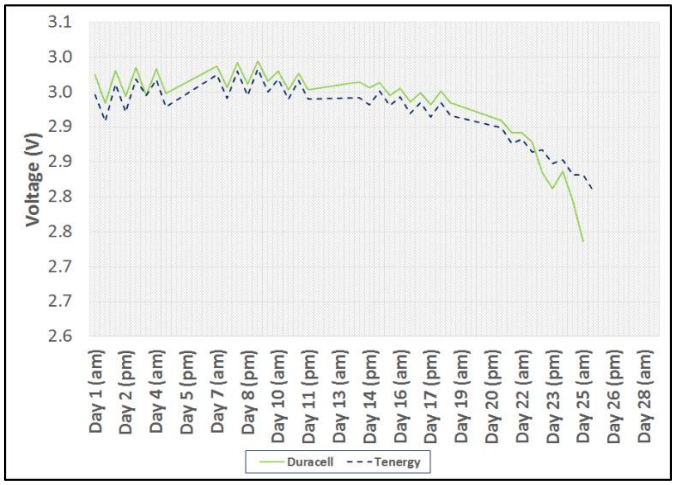

Fig. 22 Test 4 CR2 Voltage vs Time (days)

Figure 13 and Figure 14 shows the discharge at 0ºC for a period of 28 days (test 4). The discharge of the CR2 batteries is shows in Figure 13 where both had a common behavior. Figure 14 shows the discharge of the rechargeable batteries (both batteries with same behavior at a constant voltage, after 3.8V through 3.7V).

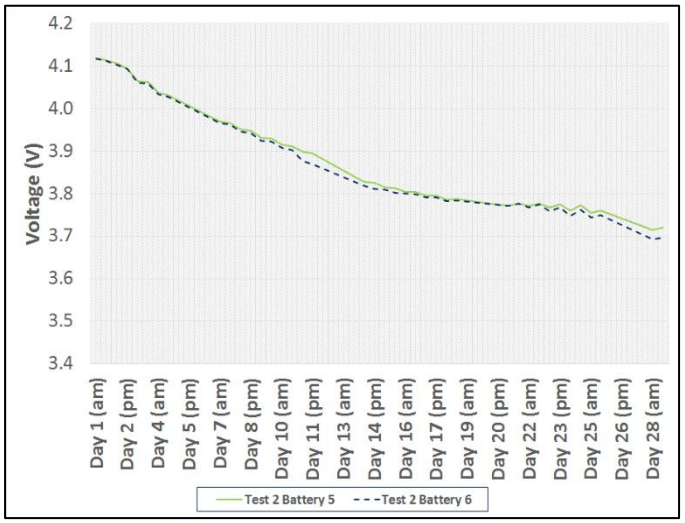

Fig. 23 Test 4 Rechargeable Voltage vs Time (days)

III. Result

Test 1 at high temperature of 50°C showed on batteries CR2 different results. Duracell battery kept a constant voltage while the Tenergy battery had a voltage difference from its first day to the second. Besides was observed physically changes on Tenergy battery like mild acid spill and casing broke off. Even with these results, this test requires more time to see the behavior until the total discharge to bring both batteries to temperature limit as manufacturing datasheet specified. The two rechargeable batteries samples shows even gradual discharge but not final, varying with the chart reference [5].

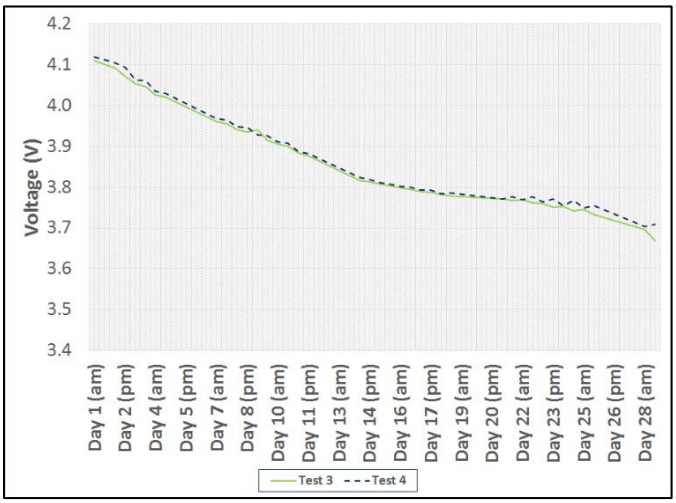

Fig. 24 Rechargeable Test 3 and Test 4 Comparison

Test 2 at a temperature of -20°C, as in test 1, shows that CR2 Duracell battery is more durable in terms of voltage and there was no inconsistency in the data after the 96 hours. Tenergy CR2 battery had a voltage discharge the first day and the following days remained constant. Rechargeable batteries maintained their voltage below the test data 1 and a ratio equal discharge.

Rechargeable Li-ion batteries were discharged faster at a lower temperature of around 0 ° C as seen in Figure 15. The behavior of the two rechargeable batteries in test 3 was as expected. Batteries began to discharge quickly and then constant, and at the end a prominent discharge. In CR2 batteries, Duracell battery remained a constant voltage while the Tenergy clearly discharge at half of the day trials.

IV. Future Works

Tests 1 and 2 could be repeated with longer periods to achieve a full discharge and see better their behavior. There will be a new test that counted with a motor vehicle where the two models of batteries (rechargeable and CR2) will be exposed to high temperatures, to analyze the discharge process in a new module of Gardien system. A simulation in COMSOL Multiphysics program would be helpful to verify the behavior of the discharge process.

References

[6] Statistics. (2016). Retrieved July 10, 2016, from http://www.kidsandcars.org/media/statistics/

[7] Uclés, J. A. (2015, July 31). NHTSA and Safe Kids Worldwide encourage parents and caregivers to take proactive steps in preventing child heatstroke in hot vehicles. Retrieved July 10, 2016, from http://www.nhtsa.gov/About NHTSA/Press Releases/2015/nhtsa-kids-in-hot-cars-07312015

[8] MYPIN® Universal Programmable Digital Adjustor PID https://www.amazon.com/Programmable-Thermostat-Temperature-Controller-Comsumption/dp/B00X5EZXV4/ref=sr_1_10?ie=UTF8

[9] 3D Plastic Filament - Afinia 3D Printer. (n.d.). Retrieved April 17, 2016, from http://afinia.com/3d-printers/3d-plastic-filaments/

[10] Linden, D., & Reddy, T. B. (Eds.). (1995). *Handbook of batteries* (3rd ed.). New York: McGraw-Hill.

Variants of Sorghum as Substrate for Lignin Degradation by Bacteria

Tiffany Del Valle-González[1], Solimar García-Torres, Jayleen Díaz-Mercado, MS[2], and José R. Pérez-Jiménez, PhD[3]
[1]Universidad del Turabo, Gurabo, Puerto Rico, USA, tdel22@email.suagm.edu, sgarcia77@email.suagm.edu,
[2]Universidad del Turabo, Gurabo, Puerto Rico, USA, jdiaz534@email.suagm.edu, [3]ut_jperezjm@suagm.edu

Abstract*– Lignin is a recalcitrant heteropolymer found in the cell wall of plants to confer structural strength and delay biodegradation. It is the most abundant constituent of plant debris and biomass with potential application a source for biofuel. Several fungal genera and few bacterial taxa are known to degrade lignin. Lignin partition can release highly energetic components embedded in the plant biomass not used as food source. Forage sorghum (*Sorghum vulgare*) is considered a potential energy crop due to its reduced lignin contents, grow under adverse conditions, and demands simple treatments. The main hypothesis is if mesophilic lignin-degrading bacteria can grow in variants of sorghum as the only carbon source, then lignin thermal treatments could be replaced. The specific aim for this project is to study the growth response of various lignin-degrading bacteria to various components of sorghum as sole carbon source. Lignin-degrading bacteria were isolated from soil at Universidad del Turabo, and water at the San Juan Bay Estuary system, both in Puerto Rico. Sorghum components (leaves and fresh stem) were added independently, as sole carbon source, to mineral base liquid and solid media. Growth was demonstrated qualitatively by colony biomass on solid media and quantitatively by optical density on liquid media. Twenty bacterial strains capable of lignin deconstruction were isolated. Partial sequencing of the 16S rRNA genes resulted in Lysinibacillus sp. and Acinetobacter sp. as closest homologous. Fresh inner stem sorghum resulted on more biomass than other substrates.

Keywords—lignin, biodegradation, and sorghum.

I. Introduction

Renewable energy sources consider the use of biomass for biofuel production. Despite using edible sources, plant biomass waste can be subjected to microbial processes for ethanol production. The major challenge resides on overcoming structural and chemical complexities enabled by lignin. More approaches that are current relay on thermal process that consume energy. Bioprospecting searches for mesophilic microbes that can deconstruct lignin to expose other component more readily for microbial actions. Emphasis is placed on bacteria because unicellular entities are easier to manage for optimal industrial uses of lignin deconstruction.

Lignin is one of the most recalcitrant, stable and structurally complex carbohydrate in nature [1]. The lignocellulose material of plant consists of three main fractions: cellulose, hemicellulose and lignin [2]. Lignin contributes to structural integrity and strength to plants but its separation from cellulose fraction has been a challenge for microbes [3]. In soil, few microorganisms are capable of deconstructing complex lignin polymers. Fungi are considered the main lignin degraders, such white rot fungi, *Agaricus* sp., *Phanerochaete chrysoporium*, *Pleurotus eryngii*, *Trametes trogii*, *Fusarium proliferatem*, *Erwenia* sp., *Copricus* sp., and *Mycema* [4]. Lignin degradation has been reported for several bacteria, including *Pseudomonas putida*, *Rhodococcus jostii* [5], and *Streptomyces viridosporus* [6]. Lignin breakdown releases phenolic compounds that can be measured by absorbance due to their aromatic ring [7]. Bacterial deconstructing species are expected to be more advantageous than fungi for biotechnological applications due to their manageable large-scale growth, molecular genetics, and protein expression [8].

Forage sorghum (*Sorghum vulgare*) is considered a potential energy crop due to its reduced lignin contents; grow under adverse conditions, and demands simple treatments [10-12]. It has been subjected to manipulations for decrease of lignin and increase of cellulose content. The relative content varies among life stages and structural portions of the forage sorghum. This study investigates the response of lignin-degrading bacteria to various type of sorghum.

II. Methods

Strains. Lignin degrading bacteria were isolated from soil at Universidad del Turabo (Gurabo, Puerto Rico) and from water column in the San Juan Bay Estuary system. Samples were inoculated on liquid medium (2 g of peptone, 2 g of yeast extract, and 0.5 g of Remazol Brilliant Blue R per liter). Tube exhibiting a change in color, suggests laccase enzymatic activity for lignin deconstruction, were subjected to further purification in general media (tryptic soy agar). Laccase activity was confirmed by cultivation of isolates in the Remazol Brilliant Blue R media and lignin media on multiwell plates. Isolates were initially described by Gram stain and catalase test.

Sorghum utilization assays. Mineral media was enriched independently with lignin (2% w/v), fresh inner stem sorghum (1% w/v), and senescent leaf sorghum (1% w/v) as sole carbon source. Both, fresh and leaf sorghum, were macerated for the use of the media. Qualitative utilization of sorghum was determined by growth on plates. The pH was measured on plates before inoculation and after growth. Plates were inoculated on two streak line on the surface of the medium and incubated for a week at room temperature. Growth was observed daily. Quantitative utilization of sorghum was determined by optical density on liquid media independently containing lignin, fresh inner stem sorghum, and senescent leaf sorghum (1% w/v each). Absorbance, at 600 nm wavelength, was measured on Spectronic 20 to triplicates for a period of 6 hours the day

inoculated. Then, the absorbance was measured for 5 days after the day inoculated.

Molecular characterization. DNA extraction was done for the thirty-two preliminary strains using proteinase K. Then by the Polymerase Chain Reaction (PCR), the 16S rRNA genes were amplified with 27F and 1525R primers. Amplicons were partially sequenced with primer 519R using Genetic Analyzer ABI3130. The closest homologous were determined using in BLAST.

III. RESULTS AND DISCUSSION

Strains. Partial screening of lignin-degrading consortia resulted, out of thirty-two isolates, in only twenty positive for lignin degradation (Table 1). Among them, sixteen were gram-positive rods, one gram-negative rod, two gram-positive coccus, and one gram-negative coccus. On the catalase test, only two were negative and the rest were positive. This indicated that only eighteen strains have the catalase enzyme to breakdown the hydrogen peroxide.

TABLE 1. Lignin degradation among studied strains.

Strain	Lacasse enzyme	Commercial lignin
UT0103		x
UT0105		x
UT0216	x	x
UT0218		x
UT0223	x	x
UT0279	x	
UT0327	x	x
UT0329	x	
UT0334	x	
UT0436	x	x
UT0659		x
UT0660		x
E002	x	x
E003		x
E004		x
E006	x	
E006-P2	x	
E012	x	x
E014	x	
E015		x

Evidence of Lignin breakdown. With the aim of confirmed lignin degradation by the twenty strain, a 24 well plates assay was prepared. The vertical lane on the left side was occupied by positive controls. On top of this lane was located the medium without inoculation that helped identify the changes that occurred, using this method for comparison. On Fig. 1a, it is illustrated a 24 well plates with the medium of Remazol Brilliant Blue R. The upper picture presents the well plates recently inoculated with eighteen isolated cultures from the soil samples of the Universidad Del Turabo and the image underneath shows the effects from one week later. Based on the results, by the second day of observation only two strains changed color to a darker blue and the rest remain the same. The strains began to change drastically between the third and fourth day of observation presenting a variation of colors such as purple, dark blue, gray, beige and greenish yellow. After a week, the well plates showed growth and positive results, as illustrated on the bottom image of Figure 1a. This outcome indicates that all the strains contain laccase-type enzymatic activity. This extracellular enzyme catalyzes the oxidation of various phenolic substrates found in lignin structure [6].

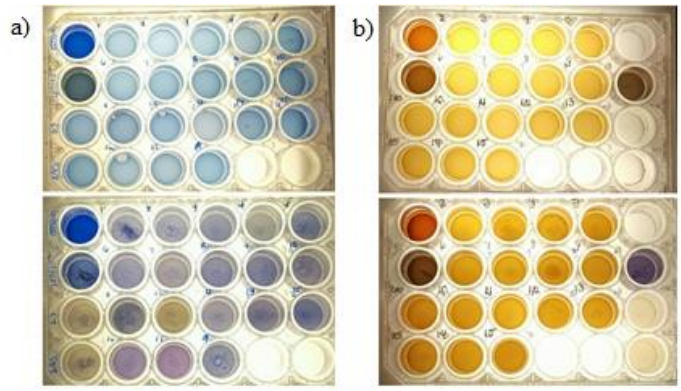

Fig. 1. Evidence of lignin breakdown on Remazol Brilliant Blue R media (a) and commercial lignin (b) as a carbon source inoculated with strains.

Figure 1b shows two 24-wells plates with lignin as the only source of carbon. The illustration from above displays fourteen strains freshly inoculated from San Juan Bay estuary and the bottom picture presents the results after a week of observation. According to the results, by the first two days, substantial growth appeared on half of the samples and only two additional demonstrated a shift in color. The next three days, the strains exhibited a change of colors including red, orange and yellow. Only two revealed negative results. The outcome shown at the bottom of Figure 1b indicates remarkable growth through the presence of turbid positive results, which stands for the capability of lignin degradation.

Sorghum utilization assays. Qualitative utilization assays were inoculated with the twenty strains (Fig. 2). Only eight strains grew in all the three different lignin sources: UT0103, UT0105, UT0216, UT0223, UT0334, UT0436, UT0659, and UT0660. Eight strains grew in lignin media and not sorghum: UT0103, UT0105, UT0216, UT0223, UT0334, UT0436, UT0659, and UT0660. All the bacteria were capable to grew in the senescent leaf sorghum and fresh inner stem sorghum containing media. The fresh inner stem sorghum resulted in the highest biomass growth.

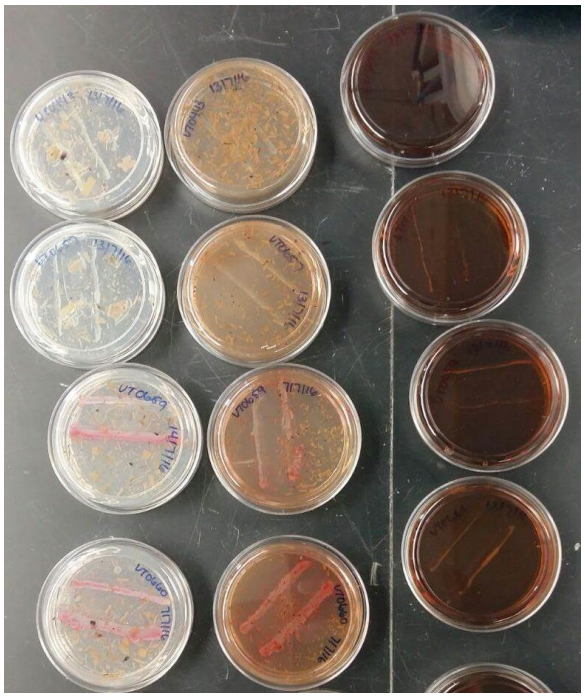

Fig. 2 Qualitative sorghum utilization assays.
Media containing fresh inner stem sorghum (left), senescent leaf sorghum (center), and commercial lignin (right).

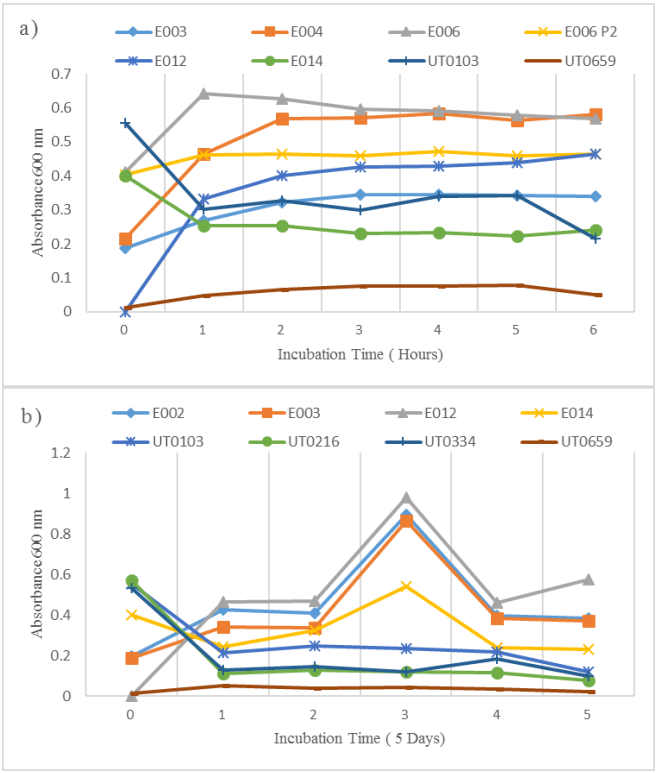

Fig. 3 Quantitative utilization of lignin by hours (a) and days (b).

The pH was measured in the culture media before and after strains grew. The initial pH 6 became neutralized after growth. In the senescent leaf sorghum media, only UT0327, UT0329, UT0334, and UT0660 neutralized the medium. The strains E002, E012, E014, UT0334, and UT0660 were capable to neutralized the fresh inner stem sorghum medium. Only UT0334 and UT0660 neutralized the three media.

Optical Density. During this experiment, optical density was used to observe the bacterial viability with three carbon sources under study: commercial lignin, fresh inner stem sorghum and senescent leaves sorghum. Absorbance measure the amount of light absorbed by culture medium and it can help us to demonstrate if the microorganism can survive in this environment. A decrease in absorbance indicate increment of soluble phenolic and polyphenolic compounds [7].

Commercial lignin as illustrated in Figure 3a displays that the microorganisms did not have a significant change in a period of six hours after the inoculation. During this interval the absorbance was constant. In three days, strains E014, E012, E003 and E002 demonstrated a high optical density as shown in Figure 3b. These changes include a decrement in the absorbance of UT012 and UT0334. The strain UT0659 did not had a significant change in this medium.

On fresh inner stem sorghum enrichment (Fig. 4), the absorbance increased right after the inoculation. In the first hour (Fig. 4a), all strains obtained an increment in their optical density. Nevertheless, strains UT0659 and UT0334 had a notable increase in their absorbance at the fifth hour. The strain UT0279 did not showed a meaningful change of the optical density. In five days (Fig. 4b), an elevation of the absorbance occurred specially in the second day of the lecture. The strains UT0659, E015 and E012 were the microorganisms that displayed more impact on this medium. However, UT0218 and UT0279 had a rise on the second day but then the absorbance was reduced. The strain UT0279 has a notable reduction because its absorbance always kept resulting negatives except day number two.

In addition, the senescent leaves sorghum enrichment demonstrated a good performance during the first six hours after the inoculation. Strains E002, E004 and E006 (Fig. 5a) shows an elevation of the absorbance during the first four hours. However, an increment of the optical density of the strain E006-P2 with an absorbance of 0.676 at the fifth day (Fig. 5b). The first read for the strain E006-P2 was -0.096, presenting that this microorganism prefers this medium more than other strains.

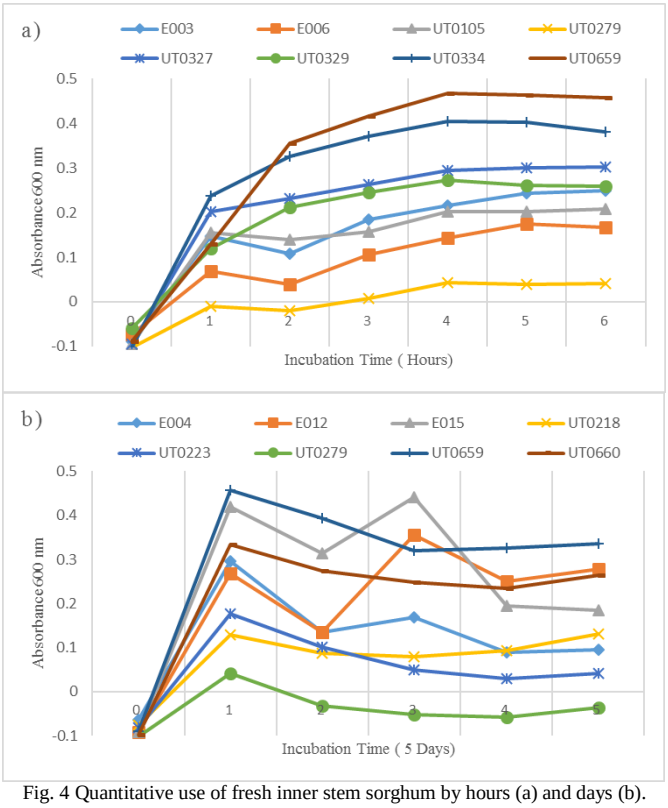

Fig. 4 Quantitative use of fresh inner stem sorghum by hours (a) and days (b).

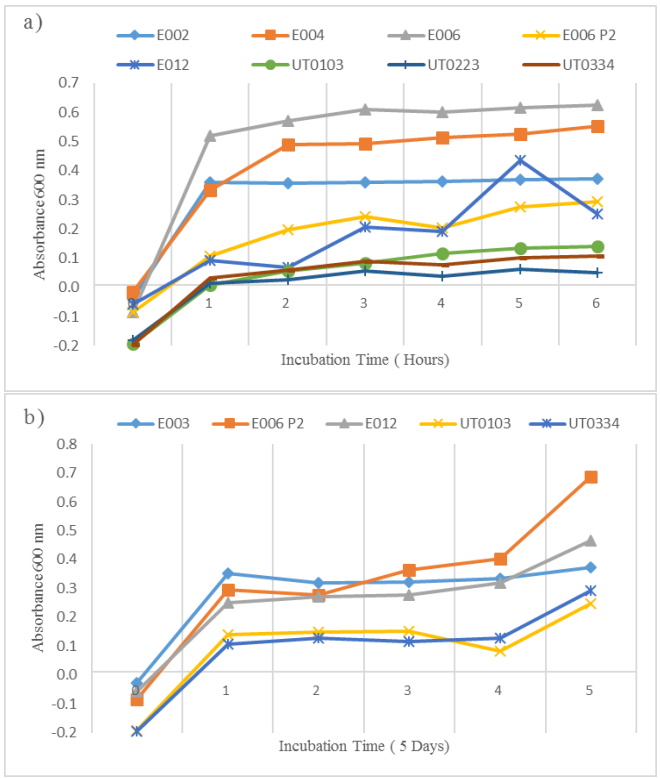

Fig. 5. Quantitative use of senescent leaves sorghum by hours (a) and days (b)

Molecular characterization. Initial attempts for molecular characterization resulted in ~400 bp sequence of the 16S rRNA genes for five strains. It is not enough to infer identity. The closest homologous were found in the genera *Acinetobacter* for strain UT0327, *Bacillus* for UT0218, *Lysinibacillus* for UT0102 and UT0105, and *Raoultella* for UT0334. All these genera have been associate to lignin deconstruction in some form.

IV. Conclusion

Microorganisms that can degrade lignin have been a remarkable challenge for microbiology due to its varied molecular structures. On previous studies, several fungi showed their ability to degrade lignin component but also there are few bacteria that can break down lignin too. The main goal of this study was to isolate lignin-degrading bacteria and create a mineral forage sorghum medium in the laboratory to replace commercial lignin. Thirty-two strains were isolated but only twenty showed positive results on well plates test with commercial lignin and Remazol Brilliant Blue R. Moreover, the results of optical density with lignin source displayed a significant change because of only eight strains four of them obtained an increment in their absorbance. Strain E006 P2 demonstrated a high performance on leaves sorghum medium compared with commercial lignin and fresh sorghum media. Furthermore, in mineral plates, a great biomass was obtained in fresh sorghum medium. In conclusion, our goal was fulfilled because a new mineral culture has been created in the laboratory. All strains achieved an amazing outcome on mineral fresh sorghum plates rather than in commercial lignin plates where it did not have a visible growth. For future studies it could be investigated which are the components of the fresh sorghum and why bacterial strain had a better development in this environment.

Acknowledgment

We are grateful to Puerto Rico Energy Center for the opportunity to work on their 2016 Summer Internship. Puerto Rico LSAMP Senior Alliance (2014-2019): Expanding Opportunities for Underrepresented College Students in 2-and 4-year STEM Programs (NSF HRD-1400868) provided partial support to TdVG. The bioprospecting component was supported by PRIMER Tropical Bioprospecting Venture for Agricultural Innovation Grant no. 2015-38422-24076 from the USDA Hispanic-Serving Institutions National Program to JRPJ. Sorghum samples were provided by Dr. Hugo Cuevas (Research Geneticist-Plants; Agricultural Research Service, United States Department of Agriculture, Mayaguez, PR). We appreciate the collaboration received from Yomarie Bernier-Casillas, Karleen González-Rosario, Karin Millán, Jonathan Otero-Colón, Francisco Rivera, and Rafael Rodríguez. Research compliance achieved according to protocols B03-007-13, B03-008-13, B03-013-13, and B03-070-16.

References

[1] J. Pérez., D.R. Rubia, J. Martínez, and A. Kapley, "Biodegradation and biological treatment of cellulose, hemicellulose and lignin: An overview" *International microbiology: the official journal of the Spanish Society for Microbiology*, vol. 5, no. 2, pp. 53-63, April 2002.

[2] V. Sasikumar, V. Priya, C. Shankar, and D. Sekar, "Isolation and Preliminary Screening of Lignin Degrading Microbes" *Journal of*

Academia and Industrial Research, vol. 3, no. 6, pp. 291-294, November 2014.
[3] K.M. DeAngelis, M. Allgaier, Y. Chavarria, J.L. Fortney, P. Hugenholtz, B. Simmons, and T.C. Hazen, "Characterization of trapped lignin-degrading microbes in tropical forest soil" *PLoS One*, vol. 6, no. 4, pp. 1-9, April 2011.
[4] M. Alexender, "Introduction to soil microbiology". 2 Ed. 1977, Kriegerpublishing company.
[6] T.D. Bugg, M. Ahmad, E.M. Hardiman, and R. Rahmanpour, "Pathways for degradation of lignin in bacteria and fungi" *Natural product reports*, vol. 28, no. 12, pp. 1883-1896, May 2011.
[5] M. Ahmad, J.N. Roberts, E.M. Hardiman, R. Singh, L.D. Eltis, and T.D.H. Bugg, "Identification of *DypB* from *Rhodococcus jostii* RHA1as a lignin peroxidase" *Biochemistry*, vol. 50, no. 23, pp. 5096-5107, May 2011.
[7] M. Ahmad, C.R. Taylor, D. Pink, K. Burton, D. Eastwood, G.D. Bending, and T.D. Bugg, "Development of novel assays for lignindegradation: comparative analysis of bacterial and fungal lignin degraders". *Mol Biosyst*, vol. 6, no. 3, pp. 815-21, May 2010.
[8] C.R. Taylor, E.M. Hardiman, M. Ahmad, P.D. Sainsbury, P.R. Norris, and T.D. Bugg, "Isolation of bacterial strains able to metabolize lignin from screening of environmental samples", *Journal of applied microbiology*, vol. 113, no. 3, pp. 521-530, May 2012.
[9] A. Thanapimmetha, K. Vuttibunchon, M. Saisriyoot, and P. Srinophakun, "Chemical and microbial hydrolysis of sweet sorghum bagasse for ethanol production" *In World Renewable Energy Congress*, no. 057, pp. 389-396, May 2011.
[10] C. Vargas. "Valoración nutricional y degradabilidad ruminal de genotipos de sorgo forrajero (*Sorghum* sp.)" *Agronomía Mesoamericana*, vol. 16, no. 6, pp. 215-223, August 2005.
[11] G. Sarath, R.B. Mitchell, S.E. Sattler, D. Funnell, J.F. Pedersen, R.A. Graybosh, and P.V. Kenneth, "Opportunities and Roadblocks in Utilizing Forages and Small Grains for Liquid Fuels" *Journal of Industrial Microbiology & Biotechnology*, vol. 35, no. 5, pp. 343-354, January 2008.
[12] B.S. Dien, G. Sarath, J.F. Pedersen, S.E. Sattler, H. Chen, D.L. Funnell-Harris, and M.A. Cotta, "Improved sugar conversion and ethanol yield for forage sorghum (*Sorghum bicolor* L. Moench) lines with reduced lignin contents" *BioEnergy Research*, vol. 2, no. 3, pp. 153-164, August 2009.

Characterization of Commonly Available Diesel Fuels in Puerto Rico

Jonathan Martínez Pacheco[1], Amaury Malavé Sanabria, PhD[2]
[1]Universidad del Turabo, Puerto Rico, USA, jmartinez471@email.suagm.edu,
[2]Universidad del Turabo, Puerto Rico, USA ajmalave@suagm.edu

***Abstract*– Five different fuel brand samples from gas stations in Caguas and Gurabo were analyzed for fuel efficiency and emissions. Approximately, 4 liters of each diesel fuel were used per test. Measurements were performed using a GUNT CT-110 7.5 KW air cooled diesel single cylinder test engine. Engine mechanical power and fuel consumption were measured using the engine test stand. Additionally, an E Instruments 4400 Portable Combustion Gas Analyzer was used to record exhaust emissions present in the combustion products, with special interest in NOx and SOx emissions. Lastly, viscosity and density tests were also performed. Results showed small variations (up to 10%) in both fuel efficiency and emissions. Results will be used as a baseline to test locally generated biofuel blends and quantify its potential as an alternative fuel.**

Keywords: combustion, efficiency, emissions

I. INTRODUCTION

Diesel fuel is a refined from crude oil, which makes it a distillate fuel considered a reliable source of energy for creating electricity and transportation methods such as trucks, buses, boats, etc.. Particularly, such methods contain diesel engines known for their low fuel consumption, durability, and reliability in commercial and industrial processes. Yet, how does the diesel combustion happen in engines? First of all, diesel ignition occurs without spark as a result of inlet air mixture and fuel injection compression. Then, the piston continues to move closer to top dead center, the mixture temperature reaches the fuel's ignition temperature, causing ignition of some premixed quantity of fuel and air. [1]

Although diesel engines convert chemical energy into mechanical energy to generate power, it also combusts/releases chemicals into the environment. Unfortunately, the majority of these chemicals are harmful pollutants, including high emissions of nitric oxide and matter emissions. [1] However, many of the emissions may vary due to its fabricant and quality, requiring for a sample to be taken out of the whole population. In this case, there is a constant doubt or observation in Puerto Rico of which diesel fuel brand/seller is the best alternative for consuming in daily tasks that require it (electrical power production, merchandise transportation, etc.) Such comparison would be determined through the analysis of combustion in a diesel engine.

II. METHODOLOGY

First of all, five different fuel brand samples (Total, Puma, Gulf, Toral, and Shell) were bought/taken from gas stations in the Gurabo area in Puerto Rico. These were acquired around the same time period of day and stored separately using a DOT approved containers. Approximately, 4 liters of each diesel fuel were stored and used per test. The test stand used for a single cylinder engine used for the tests was a GUNT CT-110 7.5 KW. Specifically, this engine was a GUNT CT-100.22 air cooled diesel engine (Figure #1). In addition, an E Instruments 4400 Portable Combustion Gas Analyzer was used to record exhaust/emission chemicals found such as Nitric Oxide (NOx) and Sulfur dioxide (SO_2). Lastly, diesel viscosity tests were taken using a Cannon 75 viscometer and density was recorded with a digital balance/pippete and a small beaker.

Fig. 1 GUNT CT-100.22 air cooled diesel engine

III. PROCEDURE

1. Test stand container was filled with Puma brand diesel to be tested, lid was fully closed after inserting the fuel extraction pump.

2. Then, the test platform, the gas analyzers and the computer software were turned on. The fuel cylinder tank was filled and engine is warmed up for 15 minutes with a load of 3.0 N*m (reduced to 1.3 N*m after start) and approximately 2300 rpm.

3. Once warm up is complete, every 30 seconds samples were taken until obtaining 50 samples for every diesel fuel type/brand (25 minute period). The portable gas analyzer and the CT-110 software recorded each data in its system while the INFRALYT CL analyzer displayed data on its monitor.
4. Once the Puma diesel test was complete, all data was saved directly to an Excel file. Note: Steps 1-4 were repeated for the other four diesel brands (Total, Shell, Gulf, & Toral).

4. Lastly, viscosity and density were measured using the mentioned tools for each fuel. Collected data was then analyzed using averages of results and standard deviation to compare among the different brands and make conclusions.

Equations

Average: (1)

$$\bar{x} = \frac{1}{n}\sum_{i=1}^{n} a_i = \frac{a_1 + a_2 + a_3 + \ldots\ldots + a_n}{n}$$

Sample standard deviation (2)

$$s = \sqrt{\frac{\sum(x - \bar{x})^2}{n - 1}}$$

Density (3)

$$\rho = \frac{mass}{Volume}$$

Braking Power (4)

$$P_B = 2\pi M_B n \frac{1}{60}\frac{1}{1000} \text{ (kW)}$$

M_B Braking Torque (Nm)

Efficiency (5)

$$P_B = \frac{P_B 3600}{B H_U} 1000$$

B fuel consumption (kg/h)

H_U Thermal Power (kJ/kg)

IV. Analysis & Results

TABLE 1 Density and viscosity of fuel brands

Gas Station Brand	Power Mechanical (kW)	Fuel Consumption (kg/h)	Specific Fuel Consumption (g/kWh)	Efficiency (%)	NO_x (%)	SO_2 (%)
Puma	0.3842	0.3851	1003.4408	8.35	0.0034	0.0002
Total	0.3690	0.4054	1097.4537	7.62	0.0035	0.0002
Shell	0.3850	0.3692	961.7638	8.73	0.0039	0.0002
Gulf	0.4030	0.3658	904.3810	9.22	0.0038	0.0002
Toral	0.4229	0.4018	958.0478	8.81	0.0035	0.0002

In Table 1 we can observe a similitude among fuel brand values regarding density since diesel's theoretical density is approximately 0.800 g/cm^3. Although kinematic and dynamic viscosity are physical properties, these varied much more significantly amongst each other. Both properties could have potentially altered test trial results since viscosity by definition is the resistance a fluid has to external forces causing it to flow. In this case, the diesel engine runs through the engine's pipeline to produce power (convert chemical energy into mechanical energy in a certain period of time).

TABLE 2 Fuel Measurements

Gas Brand	Density (g/cm^3)	Kinematic Viscosity (cSt)	Dynamic Viscosity (g/cm·s)
Puma	0.8390	5.084	4.2650
Total	0.8440	4.279	3.6120
Shell	0.8210	3.971	3.2600
Gulf	0.8310	4.466	3.7110
Toral	0.8220	4.475	3.6780

Furthermore, Table 2 shows the average of all the tests made to all 5 diesel fuels. Toral produced an average of 0.4229 kW in mechanical power and approximately 9.21% in efficiency, highest among tested fuels. However, Gulf diesel had lowed fuel consumption with an average of 0.3658 kg/h, 904.3810 g/kWh in specific fuel consumption, and 9.22% in efficiency for the tested single cycle diesel engine. Specific fuel consumption is most important to consider since it is the relationship between fuel consumed and power produced in a combustion cycle. Additionally, Table 2 also indicates that NOx and SO_2 percentages remained rather similar and low after each trial. In Figures #2 and #3, efficiency and NOx percentages are displayed in accordance to each fuel's average. Efficiency percentage results present a left skewed normal distribution while NOx percentages show a rather uniform distribution.

A standard deviation analysis was performed to compare how recorded data relates among an amount of 50 samples, in this particular case. Observations indicate a close range in deviation among the majority of the calculated data except in the efficiency and specific fuel consumption where larger intervals appear. For instance, the Total diesel fuel shows an a specific fuel consumption deviation of 547.96 g/kWh and a 10.36% efficiency deviation, indicating an alteration of lectures for such above average results.

Fig. 2 Fuel Efficiency

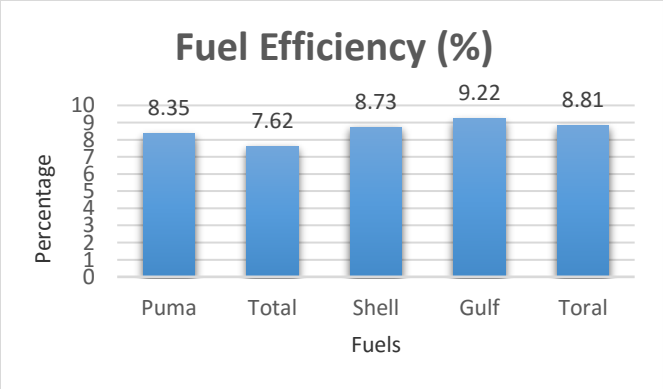

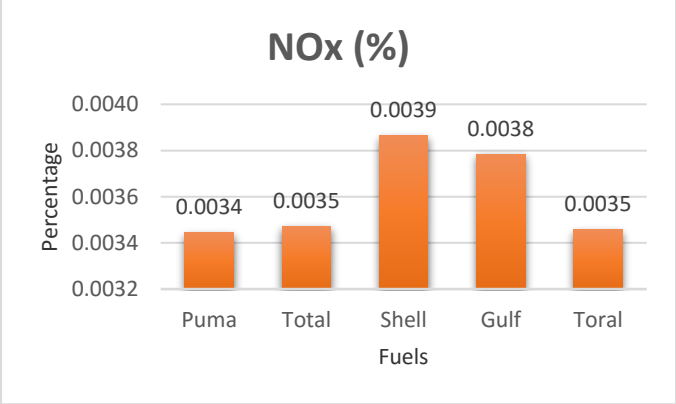

Fig. 3 NOx Emissions

CONCLUSION

Finally, after a series of observations and analysis based on each of the fuel brand samples, certain findings were considered relative when arriving at conclusions. Overall, Gulf diesel fuel was the most efficient of all since it produced the highest mechanical power and efficiency, with a fair specific fuel consumption. It also produced one of the lowest NOx and SO_2 emissions, making such fuel more reliable when considering air pollution in the environment. In this case, the worst performers were Total and Puma with the least generated power, highest specific fuel consumption and rather inaccurate precision of values when compared to the mean. For future investigations other gas station brands should be taken in consideration, as well as innovative biodiesel fuels to compare how effective the inlet (production)/outlet (emission) is regarding the fuel type. Lastly, combustion analysis should also be expanded to determine other exhaust chemicals produced by this test platform as a sample of all diesel engines.

REFERENCES

[1] Jääskeläinen, H. (n.d.). Combustion in Diesel Engines. Retrieved July 19, 2016, from https://www.dieselnet.com/tech/diesel_combustion.php
[2] Diesel Fuel Explained: Use of Diesel. (n.d.). Retrieved July 17, 2016, from http://www.eia.gov/energyexplained/index.cfm?page=diesel_use
[3] Diesel fuel Standards. (n.d.). Retrieved July 15, 2016, from https://www.epa.gov/diesel-fuel-standards

Preparation and Characterization of Bimetallic Catalysts for the Production of Synthetic Diesel

Stephanie Alsina[1], Frankie O. Rolón[1], Dayna M. Ortiz, MS[2], and Francisco Márquez, Ph. D[3].
[1]Universidad del Turabo, Puerto Rico, USA, salsina3@email.suagm.edu, frolon6@email.suagm.edu,
[3]fmarquez@suagm.edu, [2]Universidad del Turabo, Gurabo, PR, USA, dortiz23@email.suagm.edu

Abstract*– Currently, most of the world's energy comes from non renewable sources and/or fossil fuels. This generates considerable amounts of pollution causing a myriad of illnesses. The rise in fuel prices, the demand for fossil fuels and the concern for a healthier environment has made a priority the search for a viable technology to produce cleaner fuels with high commercial value. A possible source of clean fuel is synthetic diesel, which has relevance for sustainable energy. One of the most viable processes for the production of synthetic diesel is the Fischer-Tropsch (FT) mechanism, which uses synthesis gas (a mix of CO and H_2) obtained from renewable energy sources. The FT synthesis produces a mixture of linear hydrocarbons of high molecular weight and high purity obtaining synthetic fuels, such as diesel. Diesel fuel obtained with the FT process is characterized for having superior properties compared to that obtained from petroleum distillate. The objective of this research is the development of synthetic pathways for impregnation processes of bimetallic systems for the production of synthetic diesel. Synthesis of bimetallic catalysts on a SiO_2 support was executed. Silica microspheres were obtained using the Fink-Bohn-Stöber (SFB) method, at temperatures of 20.0 ˚C and 40.0 ˚C respectively. Subsequently, the impregnation process was performed with the bimetallic species (Co-Fe, Ru-Co, Ru-Fe) at concentrations of 0.025 M and 0.0050 M. The resulting materials, with different metal compositions, are promising bimetallic catalysts for the production of synthetic diesel, using CO and H_2, in the FT process. The bimetallic catalysts synthesized were characterized by both scanning electron microscopy with energy dispersive spectroscopy (SEM-EDS), and X-ray Diffraction (XRD). As a preliminary result of the achieved catalyst combinations, the bimetallic catalyst Co-Fe at 0.025 M and dispersed on the SiO_2 support at 40.0 ˚C, showed the best homogeneity (spherical shape) in its microspheres and less agglomeration between them. Relative to the average diameter, the bimetallic catalyst Ru-Fe at 0.0050 M and dispersed on the SiO_2 support at 40.0 ˚C, resulted in the smallest diameter of 0.0640 µm, compared to the other combinations. The size and distribution of the microspheres are considered important parameters which can be correlated with the expected surface area of these catalysts, and then the efficiency of synthetic diesel through the FT synthesis.

Keywords--Bimetallic catalysts, impregnation process, Stöber-Fink-Bohn method, Fischer Tropsch, synthetic diesel

I. Introduction

Nowadays, the main source of energy is that which comes from fossil fuels (i.e. oil, coal, natural gas and liquefied petroleum gas) forming an essential part in the world today. Fossil fuels attribute economic powers to countries from which it comes from and over 80% of the energy used comes from these places [1]. The development of these energy resources has led to a major expansion of energy consumption and improved quality of life for many regions of the world. However, the ever-increasing global demand for fossil fuels is causing serious environmental consequences. Today, all fossil fuel reserves that exist can reduce the oxygen concentration to less than 0.3%. The damage that these fuels make significantly influences climate change, causing air pollution, which in turn brings many diseases short- and/or long-term [1]. One of these fossil fuels is Diesel. Diesel fuel is important to the U.S. economy. As a transportation fuel, it offers a wide range of performance, efficiency, and safety features [2]. It contains between 18% and 30% more energy per gallon than regular gasoline. Diesel fuel also offers greater power density than other fuels, so it packs more power per volume. In 2015, diesel fuel accounted for about 21% of the petroleum fuels consumed by the U.S. transportation sector [2]. However, about 22.4 pounds of carbon dioxide (CO_2) are produced when a gallon of diesel fuel is burned. Carbon dioxide is a greenhouse gas that is linked to global climate change [3]. That is why, many scientists have proposed a framework for discussion on alternative energy methods that can eliminate or reduce emissions of these fossil fuels. Thus, using catalytic systems, product distribution, kinetics and mechanisms of processes, represent some of the attractive options for the production of clean fuels [6]. Presently, it has increased the interest in clean synthesis of liquid hydrocarbons, as a result of the demands of our environment, technological developments and limitations on reserves of fossil fuels.

One of the technologies for the production of these hydrocarbons is the Fischer Tropsch (FT) synthesis. This technology is used to convert sources of economic power, avoid gas flaring during oil extraction or convert raw materials such as coal and biomass to liquid hydrocarbons with higher value [7]. The FT synthesis corresponds to one of the most viable technologies being used in the production of clean liquid fuels from synthesis gas from renewable energy source; which serve to satisfy the continued demand for fuel through its use [9]. For example, diesel fuel produced by the FT process is considered more environmentally friendly than diesel derived from crude oil. It is a clean fuel, since it does not contain in its formulation aromatics or heteroatoms, such as nitrogen (N) or sulfur (S), which do not emit NOx and SOx in the combustion [8]. The design of highly active and selective catalysts for the production of such fuels with high added value, using the FT process, has experienced a boom in recent decades.

Recently, several research groups have explored the use of bimetallic catalysts to control selectivity and suppress deactivation in the reaction. Most studies using bimetallic catalysts for FT have focused on a combination of conventional transition metals, such as cobalt (Co), iron (Fe) or ruthenium (Ru). The latter shows good catalytic properties, but has a high

cost and limited availability for application in the industry. Therefore, it is necessary to maximize their efficiency in terms of activity and production of hydrocarbons, in order to make the competitive process on an industrial level with respect to the processes operating with Fe or Co [15], being the most widely used [16].

In this research, synthesis of SiO_2 with the Stöber-Fink-Bohn (SFB) method was used in an impregnation process of bimetallic catalysts for the production of synthetic diesel. These bimetallic catalysts increase the potential for selectivity and activity, improving fuel stability, since the bimetallic microspheres are highly reactive. The characterization in the synthesis of bimetallic catalysts (Co-Fe, Ru-Co, Ru-Fe) shows the microstructural parameters such as surface structure, composition, size and morphology of microspheres. Resulting in liquid hydrocarbons with low sulfur and aromatic, providing clean combustion and synthetic fuels [14].

Furthermore, the structures used as support for these bimetallic catalysts are of great importance, because they influence the dispersion, the microspheres size reduction and supported metal activity. Among the most commonly used metal dispersion media are some oxides such as Al_2O_3, SiO_2 or TiO_2 [4]. These allow to have a high metal dispersion, maximizing the available surface area and decreasing the required amount, which is of great importance for the production costs. The silicon dioxide support (SiO_2) has been successful, showing excellent conversion for this reaction [21].

The purpose of this research is for the development of synthetic pathways for the impregnation processes of the bimetallic systems, for the production of synthetic diesel. As such, a possible source of clean energy through the FT processes, in order to get a better cost/effective relation.

II. EXPERIMENTAL SECTION

1. Reactants

ACROS Organics: Cobalt (II) Chloride, 97% anhydrous; Iron (III) Chloride, 98% anhydrous; Ruthenium (III) Chloride, 99.9% anhydrous; Tetraethyl Orth Silicate, 98% (TEOS). Sigma Aldrich: Methanol, ACS reagent, ≥99.8%; Ethyl alcohol, ACS reagent 99.5%; Ammonium Hydroxide solution, ACS reagent, 28, 0-30.0% NH_3 basis; Deionized ultrafiltered water (D.I.U.F, Milli-Q). Hydrogen 5.0 (UHP).

2. Methodology

2.1 **Synthesis of Silicon Dioxide Support**

The synthesis of silicon dioxide was prepared according to the SFB method [13]. These syntheses were to developed microsphere at temperatures of 20.0 ˚C and 40.0 ˚C, in totally different processes with a reaction mixture consisting of ethanol, TEOS (the silicon source) and ammonium hydroxide. The solution at the temperature of 20.0 ˚C was executed in a 125 mL conical flask, first adding the ethanol and ammonium hydroxide. This reaction mixture was placed on a plate with magnetic stirring at room temperature, in which after reaching the required temperature TEOS was slowly added.

The reagents mixer equipment was used in the synthesis of microspheres at the temperature of 40.0 ˚C. The development of this synthesis occurred in a 200 mL round bottom flask. Then this was placed with the reactive solution ($EtOH+NH_4OH$) in a preheated heating mantle at 40.0 ˚C. For stirring, a mixer adapted to a drill was used, held to an iron support. The mixer was lowered to the appropriate depth into the flask; this method was improved to maintain the reaction under constant agitation [9]. After reaching the required temperature, a similar process at 20.0 ˚C was started, slowly adding the TEOS. The addition of TEOS at both temperatures produced a white precipitate due to the formation of SiO_2 microspheres. At the end of both procedures, the reactive mixtures were maintained in constant magnetic stirring for 1 hour. The temperature has to be always constant in every step of the synthesis [5].

After both syntheses were completed, a process of separation was conducted by centrifugation (Hermle Z-200 model) at 6,000 rpm for 10 minutes [12]. Four separation processes with deionized ultrafiltered water and one last separation with ethanol were conducted. Upon completion of the separation process, the SiO_2 microspheres were dried in an oven at 60.0 ˚C [12]. Subsequently, each of the syntheses carried were prepared for characterization of samples by scanning electron microscopy (SEM).

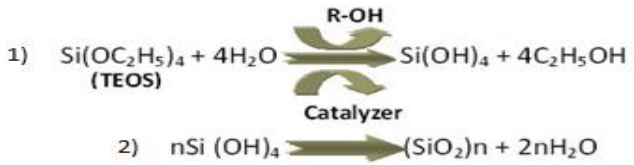

Fig. 25 Chemical process for the formation of SiO_2.

In figure 1 describes the reaction process for the formation of the SiO_2 support, the first stage of the reaction describes the controlled hydrolysis of the precursor (TEOS), this part of the reaction occurs in deionized ultrafiltered water, which is the reactant that determines the final yield of the product. The presence of ethanol in defined proportions and a catalyzer, in this case ammonium hydroxide are the determinant facts to obtain amorphous SiO_2 [15]. In the second stage a condensation process occurs to get the desired microspheres of SiO_2 [11, 12].

2.2 **Impregnation Process Bimetallic**

In this impregnation process bimetallic catalysts, such as Co-Fe, Ru-Fe and/or Ru-Co, were concentrated into 0.025M and 0.0050M solutions. In a 50 mL Erlenmeyer flask a solution of the two of the precursors of these catalysts were added: Cobalt (II) chloride, iron (III) chloride, and/or ruthenium (III) chloride [11], establishing bimetals reaction with the addition of a certain amount of SiO_2 support in the concentrations of 0.025M and 0.0050M, in completely separate processes. Then proceeded to mixing by magnetic stirring. The reaction mixture was transferred to a beaker and allowed to evaporate at 60.0 ˚C in an oven. The material was recovered and calcined in a muffle furnace, Thermolyne-Eurotherm 2116 model, in air at 300.0 ˚C for 15 minutes, and then reduced in H_2 (g) flow at 600.0 ˚C for

20 minutes in a tube furnace, Carbolite-Eurotherm 2132 model [12].

2.3 **Characterization of bimetallic Catalysts**

Once the reduction process is completed, the research concludes by characterizing the bimetallic catalysts with both SEM-EDS and XDR. These gives us information on the morphology, chemical analysis and crystal structure of the bimetallic microspheres [11].

III. RESULTS AND DISCUSSION.

A. Preliminary results of SEM for SiO_2

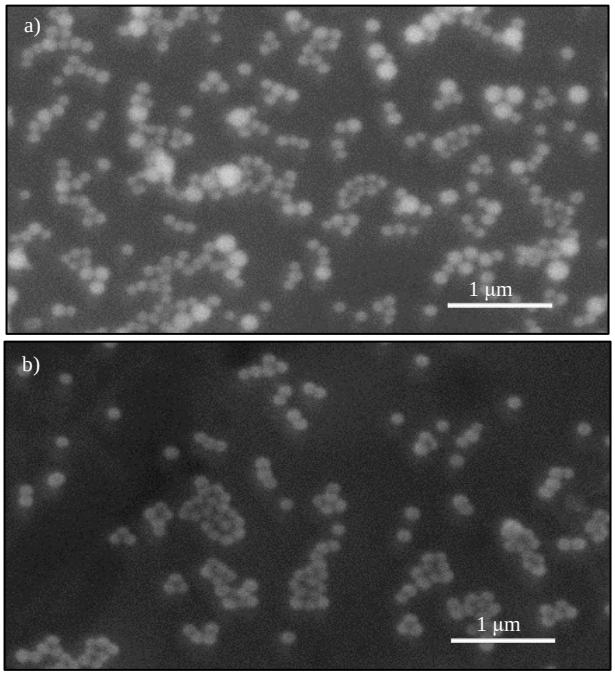

Fig. 2 (a) SiO_2 support micrograph at 20.0 ˚C; bar = 1 µm, X 20,000; (b) SiO_2 support micrograph at 40.0 ˚C; bar = 1 µm, X 20,000.

Using the method of Stöber-Fink-Bohn (SFB), samples were synthesized to obtain the SiO_2 supports at temperatures of 20.0 ˚C and 40.0 ˚C. Which after were characterized with a scanning electron microscopy (SEM-EDS), JEOL JSM-6010-LA model, available at the University of Turabo. Morphology of the SiO_2 microspheres at both temperatures (20.0 ˚C and 40.0 ˚C respectively) were observed to determine whether they were spherical or not, the degree of dispersion of the sizes and the diameters averages. In Figure 2, shows the SiO_2 support's micrographs at different temperatures, and both are at an equal magnification (X 20,000) to show the difference in size. In Figure 2 (a) 20.0 ˚C support is shown, the formation of the desired microspheres is observed. However, different sizes and small agglomeration between them is observed. This is possibly due to product formation during the reaction with the Stöber method [17]. In Figure 2 (b) the support at 40.0 ˚C is displayed, the formation of the desired microspheres with a better morphology, homogeneity in size and less agglomeration is observed between them.

The average diameter of these microspheres was determined, obtaining a measure of 0.182 µm for the temperature of 20.0 ˚C, Figure 2 (a) and a measure of 0.0554 µm for the temperature of 40.0 ˚C, Figure 2 (b). Therefore, the most suitable support for the dispersion of SiO_2 active bimetals would be the 40.0 ˚C support. This support, at this temperature, shows a lower average diameter, better morphology (spherical), and little agglomeration among microspheres. This could indicate a possible improved deposition and dispersion of the active bimetals on SiO_2 and a high value in its surface area compared to the SiO_2 support obtained at 20.0 ˚C [12-18].

B. Some preliminary results of SEM for bimetallic catalysts

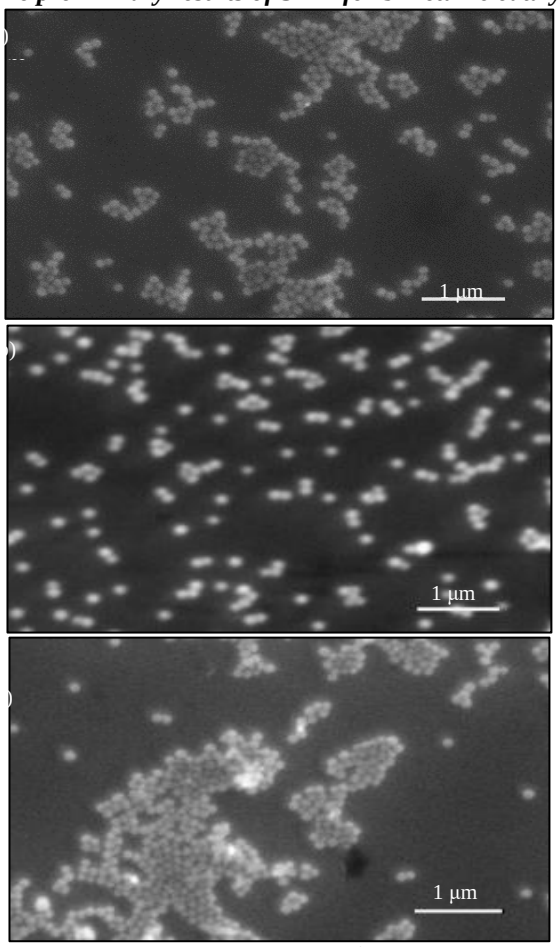

Fig. 3 (a), (b) and (c), shows the micrographs of the bimetallic catalysts on a SiO_2 supports at the temperature of 40.0 ˚C, bar = 1 µm, X 20,000

In Figure 3, shows the micrographs of the bimetallic catalysts at concentrations of 0.025 M and 0.005 M, dispersed on a SiO_2 supports at the temperature of 40.0 ˚C; after the reduction process in hydrogen flow at 600.0 ˚C for 20 minutes. In Figure 3 (a) shows the micrograph of the bimetallic catalyst Ru-Fe at 0.0050 M dispersed on the SiO_2 support at 40.0 ˚C, after being reduced; Figure 3 (b) shows the micrograph of the bimetallic catalyst Co-Fe at 0.025 M dispersed on the SiO_2 support at 40.0 ˚C, after being reduced; Figure 3 (c) shows the micrograph of the bimetallic catalyst Ru-Co at 0.0050 M dispersed on the SiO_2 support at 40.0 ˚C, after being reduced.

In Figure 3 (a) small agglomerations can be seen between the microspheres, with a defined and uniform spherical shape. The average diameter of these microspheres were approximately 0.0640 μm. In Figure 3 (b) it can be observe that there is a good dispersion in most of the microspheres, with a defined and homogeneous spherical shape and an average diameter of approximately 0.0686 μm. In Figure 3 (c) it shows that between the microspheres there are large agglomeration of the bimetallic catalyst, and a defined spherical shape. In this case, the average diameter of these microspheres were of 0.0660 μm.

As a preliminary result of the catalytic combinations made in this investigation, the bimetallic catalyst Co-Fe at 0.025 M dispersed on the SiO_2 support at 40.0 ˚C shows a better morphology (spherical shape) between its microspheres, and less compaction, which could indicate a possible better catalytic performance. Relative to the average diameter, the bimetallic catalyst Ru-Fe at 0.0050 M dispersed on the SiO_2 support at 40.0 ˚C, obtained a smaller diameter of 0.0640 μm, compared to the other combinations. On the other hand, the bimetallic catalyst Ru-Fe at 0.0050 M, dispersed on the SiO_2 support at 20.0 ˚C had the highest average diameter measuring in approximately 0.0723 μm, after the reduction process. In general, the incorporation of metals to the support generates agglomerations and inhomogeneity between particles, leading to a less defined spherical shape. This surface modification is expected to affect the specific area of the material [18-20].

*C. **Energy Dispersive Spectrometry (EDS)***

Using the Energy Dispersive Spectrometry **(**EDS) technique could determine the presence of elements in the samples analyzed. Figures 4 (a), (b) and (c), shows examples of some the spectra made in this investigation. The Figure 4 (a) shows the EDS for the synthesized sample of Ru-Fe bimetals on SiO_2 to 20.0 ˚C at a concentration of 0.0050 M; confirming the presence of Ru, Fe, Si and O in the reduced material. In Figure 4 (b) shows the EDS for the Co-Fe synthesized sample bimetals SiO_2 to 20.0˚C at a concentration of 0.025 M; confirming the presence of Co, Fe, Si and O in the reduced material. In Figure 4 (c) shows the EDS for the Ru-Co synthesized sample bimetals SiO_2 to 40.0 ˚C at a concentration of 0.0050 M; confirming the presence of Ru, Co, Si and O in the reduced material.

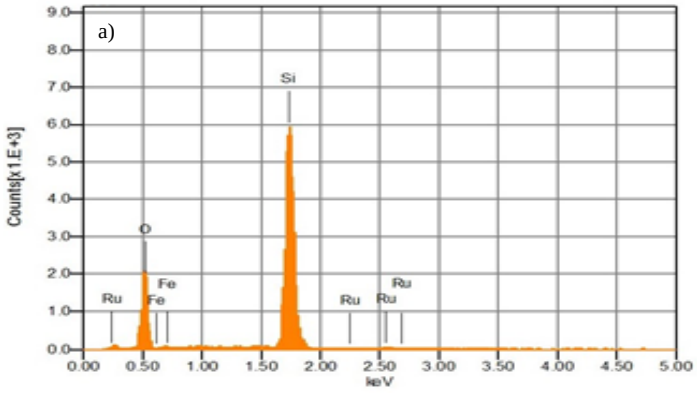

Fig 4 (a) Ru-Fe bimetals on SiO_2 to 20.0 ˚C at 0.0050 M

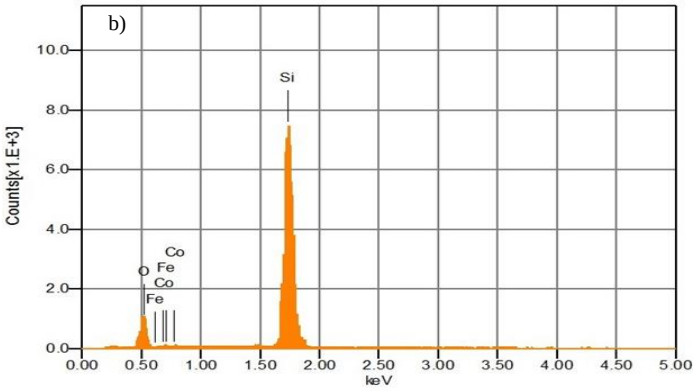

Fig. 4 (b) Co-Fe bimetals on SiO_2 to 20.0 ˚C at 0.025 M

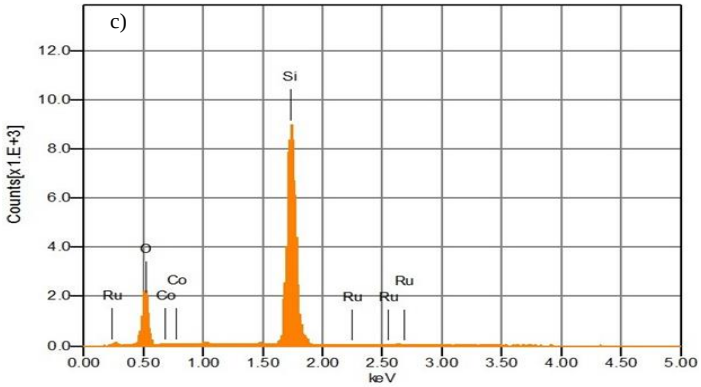

Fig. 4 (c) Ru-Co bimetals on SiO_2 to 40.0 ˚C at 0.0050 M

*D. **Some preliminary results of X-Ray Diffraction (XRD)***

Using the XRD technique, with a Rigaku Miniflex model available at the Metropolitan University (UMET), the crystal structure of the bimetallic catalysts on the SiO_2 support were analyzed. In Figures 5(a), (b) and (c), shows the diffractograms of some of the samples analyzed at 20.0 ˚C and 40.0 ˚C. Figure 5 (a) shows the diffraction pattern for the reduced sample of the Co-Fe bimetals on SiO_2 of 20.0˚C at a concentration of 0.025 M. Figure 5 (b) shows the diffraction pattern for the reduced sample of the Ru-Fe bimetals on SiO_2 of 40.0 ˚C at a concentration of 0.0050 M. Figure 5 (c) shows the diffraction pattern for the reduced sample of the Ru-Co bimetals on SiO_2 of 40.0 ˚C at a concentration of 0.0050 M. The measurements obtained in the diffractograms are very preliminary. Therefore, samples will again be characterized by the XRD process for better results.

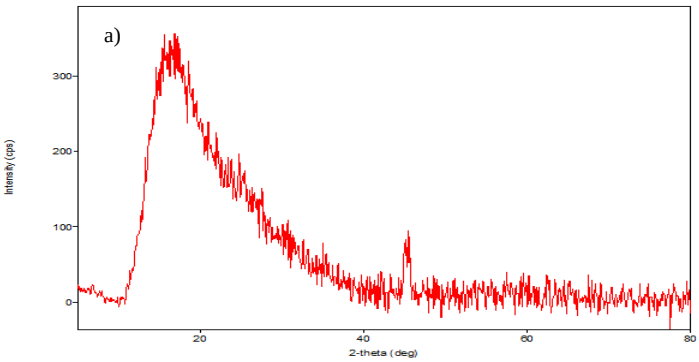

Fig. 5 (a) shows the diffraction pattern of Co-Fe bimetals on SiO_2 of 20.0 ˚C at 0.025 M.

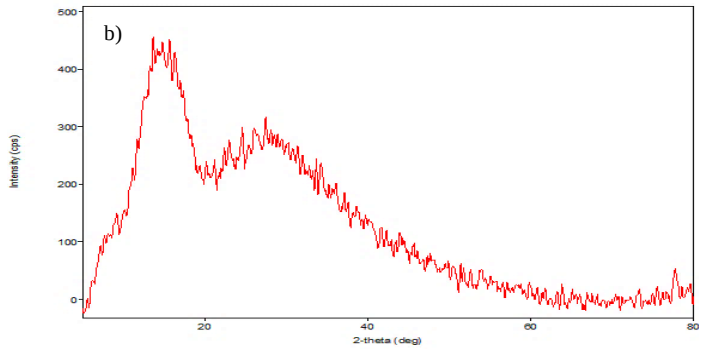

Fig. 5 (b) shows the diffraction pattern of Ru-Fe bimetals on SiO_2 of 40.0 ˚C at 0.0050 M.

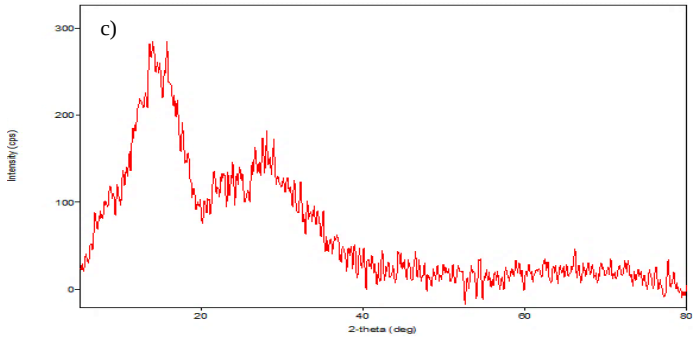

Fig. 5 (c) shows the diffraction pattern of Ru-Co bimetals on SiO_2 of 40.0 ˚C at 0.0050 M.

CONCLUSION

The result from this research about the SiO_2 microspheres were synthesized by using on the Stöber method, with certain modifications. Better results have been observed for the production of the SiO_2 microspheres when it is process without the presence of water [11]. The characterization in the synthesis of the bimetallic catalysts (Co-Fe, Ru-Co, Ru-Fe) through the SEM- EDS and XRD, shows the microstructural parameters such as surface structure, composition, size and morphology of the nanoparticles. Thus, these bimetallic catalysts for the FT synthesis are integrated to convert natural gas into liquid hydrocarbons, which makes this synthesis as one of the most viable technologies for the production of liquid fuels for the synthesis of an alternative source of renewable energy [10]. High efficiency and quality with reduced environmental, economic and social effects of fuels, with the use of renewable energy sources and/or alternative energy, are some of the most important keys to sustainable development. The significant improvement of the process requires a great technological effort, whether to improve existing solutions or seek new concepts.

ACKNOWLEDGMENT

The authors gratefully acknowledge the financial support provided by the Department of Energy through the Massie Chair project at the University of Turabo. Also, the collaboration of Abraham Garcia, Master student of the Natural Sciences and Technology; and Ian Gutiérrez, Engineer of the Puerto Rico Energy Center (PREC) for the help in the SEM-EDS study. Additionally, thanks to Dr. Mitkel Santiago of the Metropolitan University (UMET), for the help in the XRD study.

REFERENCES

[1] Armaroli, N., & Balzani, V. (2011). *The Legacy of Fossil Fuels Essay* (6th ed., 768- 784).

[2] Diesel Fuel Explained - Use of Diesel. Last updated: June 16, 2016. [Internet]. [Cited2016 Ago 9]. Retrieved by: http://www.eia.gov/energyexplained/index.cfm?page=diesel_use .

[3] Diesel Fuel Explained - Diesel and the Environment. Last updated: Last reviewed: September 23, 2015. [Internet]. [Cited 2016 Ago 9]. Retrieved by:http://www.eia.gov/energyexplained/index.cfm?page=diesel_environment.

[4] Ibrahim, I., Zikry, A., & Sharaf, M. (2010). *Preparation of Spherical Silica Nanoparticles: Stober Silica* (6th ed.). Journal of America Science.

[5] Gholami, T., Salavati-Niasari, M., Bazarganiour, M., & Noorl, E. (2013). *Synthesis and Characterization of Spherical Silica Nanoparticles by Modified Stober Process* (61st ed., 33-41). Superlattices and Microstructures.

[6] Fierro, G., Terreros, P., Granados, L., Ojeda, M., & Perez, F. (2003). *La síntesis dehidrocarburos Fischer Tropsch*. Madrid: Instituto de Catálisis y Petroleoquímica (CSIC).

[7] Gallagher, R., Boldrin, P., Combes, B., Ozkaya, D., Enache, I., Ellis, R., Rosseinsky, J. (2015). *The effect of Mg location on Co-Mg-Ru/γ-Al2O3 Fischer–Tropsch catalysts.* University of Liverpool: Department of Chemistry.

[8] Rojas, S., Ojeda, M., Herranz, T., Pérez-Alonso, F., González, J., Ladera, R. M., & Fierro, J. (2011). *Producción de combustibles líquidos sintéticos* (107(1) ed., 69-75). Química y Medio Ambiente.

[9] Araujo-Ferrer, C., Almeida, A., Zabala, A., & Granados, A. (2013). *Use of Catalysts in Fitscher-Tropsch Processes* (2nd ed., Vol. 12, 257-269). Revista Mexicana de Ingeniería Química.

[10] Hibbits, D., Loveless, B., Neuroch, M., & Iglesia, E. (2013). *Mechanistic Role of Water on the Rate and Selectivity of Fischer-Tropsch Synthesis on Ruthenium Catalyst* (52nd ed., 12273-12278). Angewandte.

[11] Arango J, Ortiz, D. Machín A, Cotto M, Márquez F. (2015). SiO_2 as catalyst support for the production of synthetic diesel, as a possible source of clean energy. PREC 2015.

[12] Márquez F, Roque R. (2005). Synthesis and characterization of silica sphere-packing mesoporous materials. Surf Int An. 37(4): 393–397.

[13] W. Stober, A. Fink and E. Bohn, (1968) "Controlled Growth of Monodisperse Silica Spheres in the Micron Size Range," Journal of Colloid and Interface Science 26: 62-69.

[14] YuYe Tong and Bingchen Tu. (2010). High Activity Bimetallic Catalyst Nanoparticles for Use in Fuel Cells. 2010-029.

[15] Calderone V, Raveendran N, Curulla D, Rothenberg G. (2011). *Bimetallic catalysts for the Fischer–Tropsch reaction. Green Chem.* 13:1950–1959.

[16] Carballo JG. 2012. Diseño de catalizadores de rutenio para la síntesis Fischer-Tropsch. [Internet]. [Cited 2014 Ago 10]. Retrieved by: https://repositorio.uam.es/handle/10486/11217.

[17] Echeverrie, M., Giraldo, F., & López, L. (2007). *Synthesis and Functionalization of Silica Nanoparticles with Spherical Morphology* (No 36 ed., ISSN 0122-1701). Universidad Tecnológica de Pereira.
[18] Marquez F., Roque R., "Synthesis and characterization of large specific Surface area nanostructured amorphous silica materials", (2006) *Journal of nanoscience and nanotechnology,* Vol 6, No 4, January
[19] Flores I., Zarazúa E., Garza L., Torres L., Valdez P, Sovolev, K., (2006) "Effect of nano-SiO_2 on properties of cement based materials", *First conference on advanced construction materials.*
[20] G, Cinti. A, Baldinelli. A, Di Michele. U, Desideri, "Integration of Solid Oxide Electrolyzer and Fischer-Tropsch: A sustainable pathway for synthetic fuel," *Aplied Energy*, 2016, pp. 308-320.
[21] Dry, M. (2002). The Fischer-Tropsch process: 1950-2000. Catalysis Today 71, 227-241.

Synthesis and characterization of carbon nanotubes using ACCVD

Tiara Polanco[1], Ariana Irrizarry[1], Luis F. López, PhD Student[2] and Francisco Márquez, PhD[2]
[1]Universidad Metropolitana, Puerto Rico, *tiarapol@yahoo.com*, airrizarry68@email.suagm.edu
[2]Universidad del Turabo, Puerto Rico, *llopez292@email.suagm.edu*, fmarquez@suagm.edu

Abstract In this study single walled carbon nanotubes (SWCNTs) were synthesized by ACCVD (Alcohol Catalytic Chemical Vapor Deposition) on silicon wafers. SEM characterization confirms the formation of SWCNTs and the feasibility of the preparation process.. The presence of aggregated particles suggested that not all nanotubes were developed because the size of the catalyst was not adequate for their formation.

Keywords- Alcohol Catalytic Chemical Vapor Deposition (ACCVD), Single Walled Carbon Nanotubes (SWCNTs).

I. Introduction

During the past few years, the nanostructured materials have aroused great interest due to its excellent properties associated with nanotechnology. These materials have generated great expectation in the fields of medicine, biology, engineering and physical-chemistry. New structures such as those of carbon and other elements of nanometric dimensions, including nanowires, nanofibers, or nanotubes have been discovered.[1]

Regarding carbon nanotubes (CNTs), many synthesis methods have been developed. The CNTs are tubular structures of nanometric diameter whose walls are formed by a network of carbon atoms in a hexagonal lattice. The denomination and the discovery of the single wall carbon nanotubes (SWCNTs) was due to S.Iijima in 1991, a few years after the discovery of the fullerenes, which are closed structures formed by carbon atoms arranged with a sp^2 hybridization.[2] A SWCNT is a closed structure derived from the "elongation" of a fullerene on a direction in such a way that its length is several times greater than its diameter, or it can be seen as a graphene wrapped and closed at its ends.[2] The SWNTs are drawing a lot of attention as materials for application in nanodevices due to its excellent electric conductivity, optical, thermal and mechanical properties that arise from its quasi-one-dimensional structure.[4]

Nowadays the synthesis of CNTs is carried out by two different methods: from graphite, through its sublimation at very high temperatures and from gaseous species through the so-called deposition of chemical species in vapor phase (CVD or *chemical vapor deposition*)[3]. The most promising alternative procedure to obtain SWCNTs is the reported by Maruyama et al. 2001[5-7,] in which a mixture of Co and Mo salts is used as a precursor of the catalyst, and the growth is achieved by means of CVD using alcohol as the carbon source.[8] This research paper presents an experimental method for the synthesis of SWCNTs, based on the ACCVD approach on silicon substrates.

II. METHODS

Preparation of substrates. The process used was described by Morant et al. 2012 for the synthesis of SWCNTs. According to this method, Co (cobalt) and Mo (molybdenum) acetate solutions are deposited on the substrate of Si by dip-coating. The catalytic solutions contain 0.0218g of Mo and 0.0437g Co in 100mL of absolute ethanol. Each solution was stirred for 2 hours and kept in the dark to avoid photodecomposition.[3] Si substrates (100) were previously cleaned with isopropanol and drying in an oven at 60 ºC for 10 minutes.[3] Subsequently the substrates were immersed in the solution of Mo by 10s and then calcined in air at 400 ºC for 20 minutes.[3] After cooling down to room temperature, the substrates were immersed in the solution of Co, following the same procedure as described above.

Growth of SWCNTs. The synthesis of SWCNTs was made using a CVD system at atmospheric pressure.[3] A quartz sample holder containing the substrates was introduced inside a tubular quartz reactor. The system was switch on, and a mixture of nitrogen (75%) and hydrogen (25%) was added with a flow of 300mL/min.[3] Simultaneously the reactor was heated to 1000 °C. (30 °C/min), and the substrates were maintained at this temperature for 10 min. At this temperature a mixture of nitrogen and ethanol (99.5% ethanol and 0.5% water) was added for 5 minutes. After that, the system was cooling down to room temperature under a flow of nitrogen.

Characterization. The synthesized samples were characterized by scanning electron microscopy using a JEOL JSM-6490LV at different magnifications. The samples were not gold coated, since these materials are sufficiently conductive.

III. Result and Discussion

The synthesized carbon nanotubes were characterized by SEM. Fig. # 1 shows a SEM image (at low magnification) of the surface of the material. As can be seen there, this image shows high density of nanotubes randomly distributed on the surface of the silicon wafer.

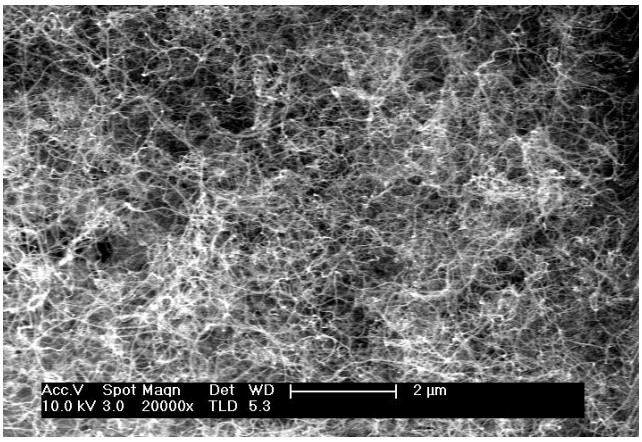

Figure 1 - SEM image at low magnification of the carbon nanotubes growth.

On the high-density areas can be observed large quantity of carbon nanotubes forming a kind of "clusters" of circular shape. As the image is magnified it is noted that this type of macrometric structures are formed individually by threads at nano scale and particles that did not completed their growth as shown in Fig. # 2A. The particles that did not complete their growth are known as "clusters". Particles similar to these, but smaller in size, are responsible for the growth of nanotubes. Only particles with ideal size (ca. 5-10 nm) are able to catalyze the synthesis of carbon nanotubes. The physical-chemical properties of materials with high density of aggregated particles may be different to those obtained with the nanotubes and, therefore, the potential applications of these materials vary or simply cannot be used for some common purpose. The formation of carbon nanotubes can have some disturbances in its development associated to factors of temperature, amount of reagent in solution, reaction time, purity of alcohol, among other factors that could affect the growth process.

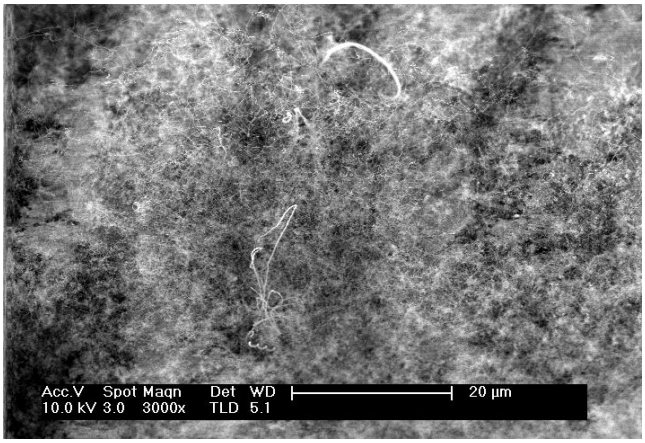

Figure 2A: SEM image showing the formation of "clusters".

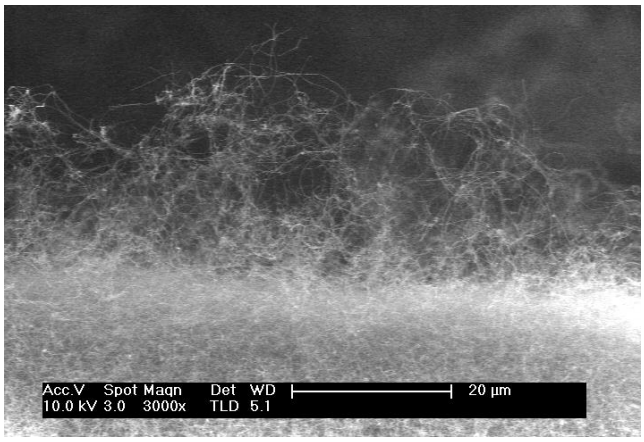

Figure 2B: SEM image corresponding to a side-view of the silicon substrate showing the carbon nanotube growth.

For future research it is necessary to use other techniques of characterization such as X-ray diffraction and Raman to achieve a better understanding of the crystalline structure of these novel materials, and to determine the nature of the carbon nanotubes.

CONCLUSIONS

The synthesis method used for the growth of carbon nanotubes was demonstrated to be effective. The presence of aggregated particles or "clusters" are indicators that not all particles reach the required sizes for the formation of nanotubes. The temperature, the amount of reagents, mixing and reaction time are determinant factors in the preparation of the carbon nanotubes.

ACKNOWLEDGEMENTS

The authors thank to the Puerto Rico Energy Center (PREC) for the use of the characterization facilities. Financial support provided by the US DoE, through the Massie Chair project at University of Turabo, US Department of Defense, under contract W911NF-14-1-0046, and from the Ministerio de Economía y Competitividad (MINECO) of Spain, through the grant ENE2014-57977-C2-1-R, are gratefully acknowledged. Finally we thank the Universidad Metropolitana and Universidad del Turabo for giving us the opportunity to conduct this research.

REFERENCES

[1]. Field, T. Synthesis and characterization of carbon nanotubes and silicon nanowires: Technological Applications. PhD Thesis, Autonomous University of Madrid, Ciudad Universitaria de Cantoblanco, is, November 2012.

[2]. Jimenez, P. Nanostructured materials based on polyaniline, carbon nanotubes and graphene. PhD Thesis. University of Zaragoza, Zaragoza, February 2011.

[3]. Morant C.; Field T.; Márquez F.; Conception D.; Elizalde E. Mo-Co catalyst nanoparticles: comparative study between Tin and Si surfaces for single-walled carbon nanotube growth. Thin Solid Films 2012, 520, 5232-5238.

[4]. Garcia, J. Hybrid systems of polyalinile and nanoestructures of carbon for its application in artificial muscles and supercapacitors. PhD Thesis, University of Alicante, Alicante, July 2012.

[5]. Maruyama S.; Kojima R.; Miyauchi Y.; Chiashi S.; Kohno M. Low-Temperature Synthesis of High-Purity Single Walled Carbon Nanotubes from Alcohol. Chem. Phys. Lett. 2001, 360, 229-234.

[6]. Murakami Y.; Miyauchi Y.; Chiashi S.; Maruyama S. Characterization of carbon nanotubes single-walled catalytically synthesized from alcohol. Chem. Phys. Lett. 2003 , 374, 53-58.
[7]. Murakami Y.; Miyauchi Y.; Chiashi S.; Maruyama S. Direct Synthesis of High-Quality Single-Walled Carbon Nanotubes on Silicon and Quartz Substrates. Chem. Phys. Lett. 2003, 377, 49-54.
[8] Márquez F.; López.; Morant C.; Roque R.; Conception D.; Elizalde E.; Zamora F. Structure and characterization of vertically aligned single-walled carbon nanotube. Nanomater Bundles. j. 2010,1-7.

Optimization of algae culture media for accelerated production of oils to biofuel

Christian Del Valle, BS[1], Jonathan López-Carrasquillo, HS[1], Karleen González-Rosario, BS[2] and José R. Pérez Jiménez, PhD[3],
[1]Universidad del Turabo, Gurabo, PR, USA, [1]delvallechristian67@gmail.com, [1]jlopez644@email.suagm.edu,
[2]Universidad del Turabo, Gurabo, PR, USA, karleen_12073@hotmail.com, [3]ut_jperezjm@suagm.edu

Abstract ***Modern life has been facing new challenges, this include the search for new technologies that doesn't depend on petroleum, because of the great damage that can cause to the planet ecosystem. Microalgae are photosynthetic microorganisms that use sunlight to create organic matter through carbon dioxide, and water, in order to easily convert solar energy into lipids. Oil produced by algae can be useful for biofuel production and can represent a better ecofriendly option. The main objective of this research is to determine the influence of nutritional composition of algae media to accelerate their production of oils by two wild algae in batch culture. Two media were prepared to satisfy salt requirements for each algae: Chlorella vulgaris and Nannochloropsis sp. Each alga was reactivated and was inoculated with two treatments: Pasta Residual Water (PRW) and Vegetable Residual Water (VRW). Measuring their optical density, we determine that PRW represent a better nutritional supply to accelerate the growth of the two algae. Continue culture will be performed in the future in order to extract the oil produced by the two algae and determine their quality and their potential use for biofuel production.***

Keywords-- Chlorella **sp., algae,** ***Nannochloropsis*** **sp.**

I. Introduction

Since the modern impact of new technologies and the exponential increase of population and their needs, there have been a lot of concerns about the great amount of technologies based on petroleum, which create a great strain on them. However, scientist have been working for new alternative that can be ecofriendly and have a better impact on the economy. Previous research has used agricultural crops, animal fat and others to satisfy the necessity of creating a new sustainable energy, but neither can really satisfy the great demand that represent the energy industry [6]. This study aims to open new doors to the scientific community about the great opportunity that can represent algae on the biofuel field. Not only this study search for an alternative biofuel but to create awareness on the environmental impact cause by petroleum. The combustion of petroleum based fuels cause a proliferation of gases; which have resulted in diverse contaminants. However, multiple studies have shown the production of biofuels by extraction of oils directly come from algae [2].

Furthermore, algae were one of many assertive resources that were taken for the production of biodiesel. Algae are a species of photosynthetic microorganisms that use sunlight to create organic matter through carbon dioxide, and water, in order to easily convert solar energy into lipids. The production of biofuels from microalgae is commercially viable as it is cost competitive with fossil fuels, does not require additional land, improves air quality by absorbing carbon dioxide in the atmosphere, and uses a minimal amount of water [1]. Nonetheless, the advantage that stands out when using algae for this study is the ability of rapid growth, and does not require the quality resources; such as cultivation conditions for obtaining an effective product. Oil productivity depends on the rate of algae growth and biomass content [2].

The success of algae oil for biodiesel has a direct correlation with algae strain [5]. Different techniques and methods that affect the species growth, has been used in order to find the best nutritional parameters for algae. It has been found that the algae biomass increase is more substantial when a homogeneous supplement is added [7]. Although, two diverse strains of algae have been recognized for potential biofuel production: *Chlorella* sp. and *Nannochloropsis* sp. *Chlorella* is a unicellular microalga that has been highlighted as one of the most studied algae species due to its conformation, and photosynthetic efficiency compared to other species. It is spherical, approximately 10 µm in diameter, and lacks flagella. *Chlorella* contains a green pigment, photosynthetic chlorophyll a and b, in its chloroplasts. It multiplies rapidly through photosynthesis, requiring only carbon dioxide, water, sunlight, and a small amount of minerals to reproduce.

Nannochloropsis sp. is a genus of algae comprising, approximately, 6 species. Most species have been known from the marine environment, but also occur in fresh and brackish water. This can represent a great opportunity because of the different capabilities on diverse conditions that needs to be tested in order to find in which condition can be the best for lipids production. All species are small and non-motile. Nevertheless, it is different from other related microalgae because it lacks chlorophyll b and c, and have a diameter of about 2 µm. *Nannochloropsis sp.* is considered as a promising alga for industrial applications due to their ability to accumulate high levels of polyunsaturated fatty acids.

Unicellular microalgae produce a cell wall containing lipids and fatty acids; which set them apart from the higher animals and plants [3]. In addition, new emerging technologies explore bacterial interactions of algae for improved growth and production of lipids in microalgae. [4].

The main objective of this research is to determine the influence of nutritional composition of algae media in the production of oils by two wild algae, with green pigments, in batch culture. Once we demonstrate that algae have a better response with the nutritional parameters that we stablish, there will be a continuous culture in photobioreactor for quantitative and qualitative assessment of the algae oil.

II. Methods

A. Media Preparation

Due to different type of salt requirement, we prepared two different media, one for *Chlorella vulgaris* and another for *Nannochloropsis sp.* Algae and media ingredients were bought to Algae Research Supply and Algae culturing kit was used to reactivate the algae. *Chlorella vulgaris* media was prepared with a bag of salts with sodium chloride, sodium bicarbonate and calcium chloride was poured into a half-liter bottle of 500 ml of drinking water until dissolved. Then, a nutrient fertilizer was added that consist of a modification of Bold's Basal Medium (BBM), it uses sodium nitrate and sodium phosphate. A culture flask was filled with 50 ml (2/3 full) of culture media and algae were inoculated. This culture was exposed to direct sunlight with occasional shake. For *Nannochloropsis* sp., a mix of salts with sodium chloride and sodium bicarbonate was poured in 500 ml of drinking water. Then a nutrient fertilizer that consist of a modification of the F/2 media, which uses sodium nitrate and sodium phosphate as the nitrogen and phosphorus sources was added to the drinking water with salts. In order to reactivate the algae, a flask with 50 ml (2/3 full) of media and algae was prepared. Indirect sunlight was given for the algae photosynthesis with occasional shake.

B. Nutritional Regimes.

In order to define the nutritional regime that promotes a better growth for algae, two treatments were applied. Each alga was inoculated in their respect media and was supplemented with Pasta Residual Water (PRW) or Vegetable Residual Water (VRW). Each supplement was collected and sterilized in autoclaved prior addition to the media. For a better understanding of the behavior of each alga, a duplicate was made for treatment. Each treatment was observed in the spectrophotometer three times each day for optical density measurement in 600nm. This data was used to plot a growth curve to demonstrate which treatment does a better effect on the algae growth.

III. Results and Discussion

Chlorella vulgaris demonstrated faster growth, based on the production of its characteristic pigment, among the two algae strains activated. Microscopically, all algal strains were pure and preserved typical morphological features. In order to determine the most stimulating substrate for growth, *Chlorella vulgaris* was cultivated in F2 mineral media (F2) supplemented with 10% of vegetable residual water or 10% pasta residual water. Growth was assessed by optical density for five days. Culture tubes allowed 40% space for atmosphere containing CO_2 (carbon source for photosynthesis) and were kept under sunlight (source of energy) and shake occasionally.

The typical growth media (F2) was supplemented with pasta residual water (10% v/v) from food processing as additional carbon source. Pasta residual water (PWR) from cooking resulted in a homogeneous solution that mixed with F2 without evident separation of phases or aggregate formation. This medium (F2+PWR) showed a gradual and smooth growth of algae biomass. Between the two replicas (Fig. 1), *Chlorella vulgaris*. follows a similar growth trend: adaptation (lag) phase in the first 40 hours, log phase slowly but consistent for about 90 hours, and later the growth became to stabilized. The medium F2+PWR conserved it homogeneity throughout all the experiment.

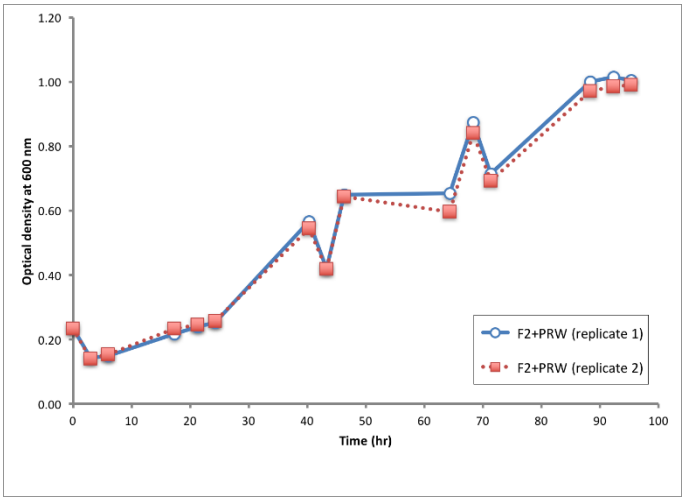

Fig. 1 Growth of *Chlorella* sp. in F2+PRW

The typical growth media (F2) was supplemented with the second treatment vegetable residual water (VRW; 10% v/v) from food processing as additional carbon source.

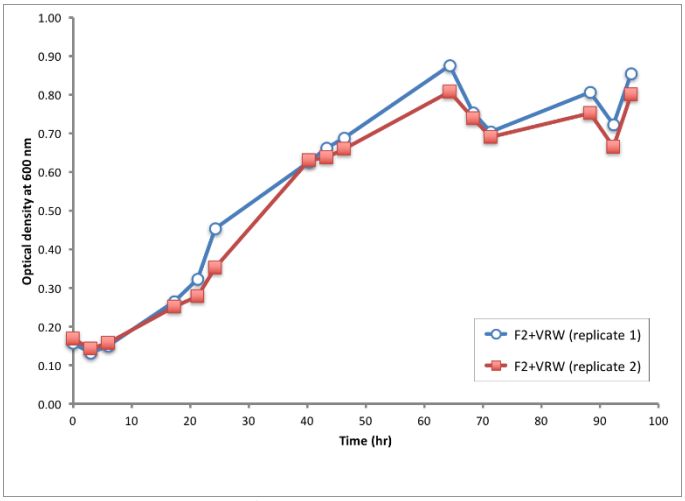

Fig. 2 Growth of *Chlorella* sp. in F2+VRW medium

Similar to the PRW, the solution resulted in a homogeneous mix with F2 without evident separation of phases or aggregate formation. This medium (F2+VRW) showed a gradual and very exponential growth of algae biomass. A similar result was observed for the two replicas (Fig. 2). *Chlorella* sp. follows a similar growth trend: adaptation (lag) phase in the first 60 hours, log phase slowly but consistent for about 70 hours, and later the growth became to stabilized. The medium F2+VRW conserved it homogeneity throughout the study.

Nannochloropsis sp. was subjected to the same nutritional regimes (F2+PRW and F2+VRW) than *Chlorella vulgaris*.

Results showed a more stable and homogeneous growth than *Chlorella vulgaris*. However, *Chlorella vulgaris* demonstrated more increment in 100 hours. Similar results were observed for the two replicas (Fig. 3). *Nannochloropsis sp*. follows a similar growth trend: adaptation (lag) phase in the first 60 hours, log phase slowly but consistent for about 90 hours, and later the growth became to stabilized. The medium F2+VRW conserved it homogeneity throughout all the experiment.

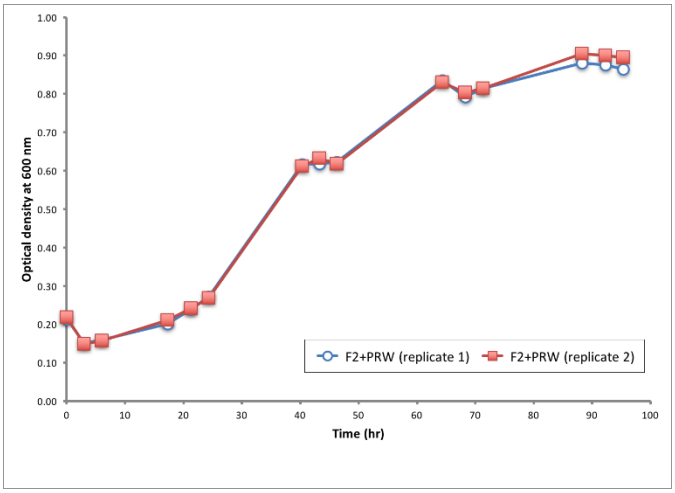

Fig. 3 Growth of *Nannochloropsis* sp. in F2+PRW medium

Ultimately, *Nannochloropsis* sp. was exposed to F2 media supplemented with VRW. Results showed a more radical and heterogeneous growth than *Chlorella vulgaris*. However, *Nannochloropsis* sp. is expected to have a better increasing than *Chlorella vulgaris* as we can see that there's not a stabilized growth which brings the opportunity that this alga in the 100 hours it's still growing. Different tendencies were observed for the two replicas, but in a final stage they showed similar tendencies (Fig. 3). *Nannochloropsis* sp. follows a similar growth trend: adaptation (lag) phase in the first 100 hours. Future research will make a more prolong read to have a better understanding of how much the VRW as carbon source can help the algae to growth.

Finally, biomass increases for both algae and nutritional regimes (Fig. 4). *Chlorella vulgaris* showed greater growth when the basal media was supplemented with pasta residual water (F2+PRW). This results prove once more that *Chlorella* species can be a better opportunity for the energy industry as previous research demonstrated that this algae strain can growth better than others strains tested using media supplemented with different carbon source [7].

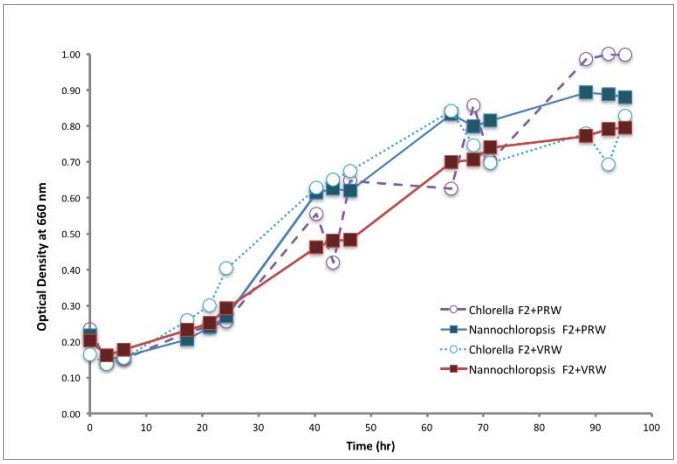

Fig. 4 Growth of algae under nutritional regimes

In the future, once significant increase in algae cell number is obtained, we can put the algae in a starvation state to stimulate the production of oils.

ACKNOWLEDGMENT

We are grateful to Puerto Rico Energy Center for the opportunity to participate on their 2016 Summer Internship. The research was supported in part by PRIMER Tropical Bioprospecting Venture for Agricultural Innovation Grant no. 2015-38422-24076 from the USDA Hispanic-Serving Institutions National Program to JRPJ. We appreciate the collaboration received from Yomarie Bernier-Casillas, Research compliance achieved according to protocols B03-007-13, B03-008-13, B03-013-13, and B03-070-16.

REFERENCES

[1] K. E. Apt, and P. W. Behrens. *"Commercial developments in microalgal biotechnology"*. *Journal of Phycology*. vol. 35, no. 2, pp. 215-226, Apr 1999.

[2] S. Behera, R. Singh, R. Arora, N. K. Sharma, M. Shukla, and S. Kumar1. "Scope of algae as third generation biofuels". *Frontiers in Bioengineering and Biotechnology.* Vol 2, pp 90. Feb 2015.

[4] R. M. Srikanth, F. Md. Y. Fatimah, S. Banerjee, and M. Shariff. "Microalgae as Sustainable Renewable Energy Feedstock for Biofuel Production". *BioMed Research International*. vol. 2015, pp. 13. 2014.

[5] G. Araujo, L. J. Matos, L. R. Gonçalves, F. A. Fernandes, and W. R. Farias. "Bioprospecting for oil producing microalgal strains: Evaluation of oil and biomass production for ten microalgal strains". *Bioresour Technol*. Vol. 102, no. 8, pp. 5248-5250. April 2011.

[6] Y. Chisti. "Biodiesel from microalgae". *Biotechnology Advances*. vol. 25, no. 3, pp 294–306, May-June 2007.

[7] J. López-Carrasquillo and J. R. Pérez-Jiménez. Nutritional Stimulation of *Chlorella sp.* in Batch Culture prior Production of Biofuel. PREC Summer Internship. 2015.

Non-destructive Structural Characterization of Reinforced Concrete Members

Alejandra M. López Morales[1], Rolando García, PhD[2]
[1]Universidad Del Turabo, Puerto Rico, alopez340@email.suagm.edu, [2]rogarcia@suagm.edu

Abstract –Puerto Rico is located in a region with high risk of seismic activity. Historically, seismic events of great magnitude occur in Puerto Rico every one hundred years. This should be concerning considering that almost a hundred years have passed since the last grave earthquake stroke the island. If an earthquake of great magnitude were to occur today, there is no doubt that many of the country's infrastructure would be affected. Specifically, creole constructions built on hills and sloped terrains. This structures usually lack of surveys and do not follow construction code guidelines. Therefore, there is basically no information on the reinforcement of these reinforced concrete (R/C) structures and members. This project is meant to give us an insight of the rebar that is used in these creole hillside houses. To achieve this the ZBL-R630A Rebar Scanner, which is considerably economic compared to high quality rebar scanners, will be used to measure concrete cover, diameter of rebar, location and spacing between rebar. The Rebar Scanner will be tested with two different concrete members that were designed with different reinforcement scenarios. These members will be R/C columns or beams. Since the exact location of the rebar is known for these members we can measure the accuracy of the ZBL-R630A. The continuous performance of test with the scanner will help us to understand it and allow us to calibrate it and determine how to obtain reliable readings.

Keywords—R/C structures, Rebar Scanner, Rebar Location, ZBL-R630A, Seismic Hazard, Creole Construction, Hillside Construction

I. Introduction

Puerto Rico is located between the North American and the Caribbean plate and south of the Puerto Rico Trench. Its location makes the island vulnerable to the occurrence of tremors and/or earthquakes. The last big earthquake that occurred in Puerto Rico was the San Fermín earthquake which stroke in October 11, 1918. This seismic event was registered to have a magnitude of 7.3 in the Richter scale causing the death of 116 people and millions in loss and damages. History shows that these events occur in Puerto Rico approximately every hundred years, meaning that our time is due.

Before the occurrence of a large scale earthquake, Puerto Rico's dated and creole structures built at hillsides would be at imminent risk. It is a common practice in Puerto Rico to build reinforced concrete frames for residential houses on hilly terrains and to support them with slender columns. Furthermore, it is common that these houses lack of good construction practices. In her study, Gonzalez [3] found that there was no reliable information about the reinforcement details in the columns of these type of structures and had to recur to use the minimum reinforcement requirements established by ACI 318-11.[1]. Similarly, in his study, Vázquez [4] found that steel reinforcement parameters of the residences were not available because the residences were old and the owners did not have construction drawings.

The first step to finding an effective remedy to the risk that hillside constructions encounter if facing an earthquake is to obtain knowledge as to their reinforcement. A rebar scanner is a detection tool that allows obtaining data of the rebar in reinforced concrete members without damaging the previously built structure (non-destructive procedure). Even though certain models of this equipment can be bought for hundreds or low thousands of US dollars, higher end models can reach up to the $60,000. The rebar locator utilized in this study was the ZBL-R630A Rebar Scanner. This apparatus is able to detect ferrous materials in concrete. It also tests the thickness of concrete cover (C.C.), rebar diameter, location and space. Furthermore, the scanner allows us to store and transfer data from tests. [2] Conducting tests and results yielded by the ZBL-R630A will give us an idea of its reliability. Furthermore, by comparing theoretical and experimental data of rebar location and dimensions will provide information on the scanner's performance and analysis.

II. Problem Statement

There is barely, if not any, information on the reinforcement of reinforced concrete Puerto Rican structures built on hillside terrain [3, 4]. This is problematic when determining the effects that seismic activity will have on these type of constructions. Currently, the way of managing earthquake loads in these structures are shear walls. These, are walls that carry earthquake loads down to the foundation. However, this solution is not always dependable. In order to develop new techniques to deal with the impact and consequences of earthquakes in hillside residences in Puerto Rico it is important to know construction details like reinforcement particulars. The study and domain of the rebar detector is key in obtaining trustworthy readings. This can later lead to locating and modeling the reinforcement of the previously mentioned structures.

III. Purpose and Scope of Work

The purpose of this research is to test the ZBL-R630A rebar locator in different scenarios that might be representative to those in residences built on hilly terrain. The analysis and comparison of the information that the tests will supply will provide understanding of the machine's performance. This

project is meant to achieve full understanding, management and interpretation of the rebar scanner and the data obtained from the apparatus. This can later be used in actual previously built hillside constructions to inspect and analyze their reinforcement. Gathering this data could lead to further understanding the effects of an event such as an earthquake in these structures. In the future, this information can help to develop new structural and economical methods to manage and prevent the hazardous effects caused by earthquakes that hillside creole constructions are at risk of suffering.

IV. Methodology

To understand the performance of the ZBL-R630A rebar scanner, it was tested with different reinforced concrete members with different types of rebar. One of the members, that was built is a concrete column/beam with dimensions of 17"x8"x8'. This sample was reinforced with one layer consisting of three rebar to each side. Each layer contains two $^{5}/_{8}$" diameter rebar and one $^{1}/_{2}$" rebar. The second specimen that was built was designed with dimensions of 12"x12"x8'. This sample's reinforcement has a diameter of $^{5}/_{8}$". To one side the reinforcement consists of one single layer. To the other side, it is double layered. Both specimens were designed to have a concrete over of $1^{1}/_{2}$" to every rebar.

The first specimen is also reinforced with fifteen steel hoops with diameter of $^{3}/_{8}$" and dimensions of 5"x14". The second specimen has 19 steel hoops of the same diameter of dimensions 9.5"x9.5". These prefabricated hoops were tied to the rebar with black construction wire. Furthermore, nylon thread was used to fix the position of suspended rebar throughout the mold. Fig. 1 and Fig. 2 show the designed displacement of the rebar and hoops in each mold for specimen 1 and 2 respectively. However, in the laboratory the steel hoops that were used had dimensional and shape irregularities. Consequently, the design parameters of all the reinforcement were altered.

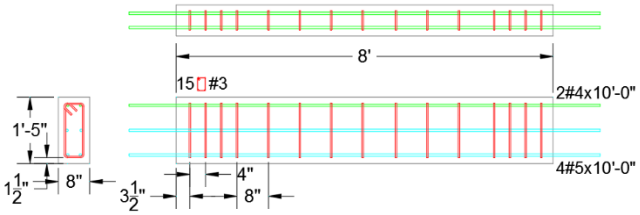

Fig.1 Top and side view of first specimen reinforcement design

Before the pouring of the concrete, the reinforcement position was recorded in the laboratory by taking various measurements. These included the estimated C.C. to every applicable side of each rebar and hoops. Also, the distance that separated each hoop and rebar from one another.

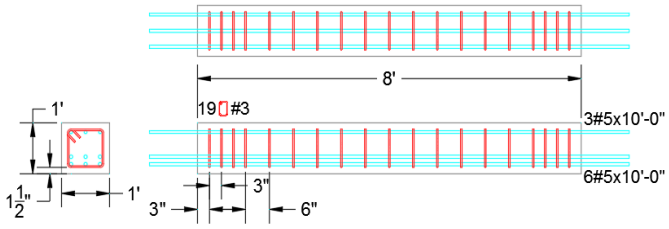

Fig.2 Top and side view of second specimen reinforcement design

The final members were built with poured concrete of 3,000 psi resistance. Due to time constraints, an additive for high early strength at 3 days was added to the mix. Furthermore, four 4" x 8" concrete cylinders were made with the mix to test in compressive strength. In the process of pouring the concrete, the mold for the 12"x12"x8' column expanded significantly. Therefore, the dimensions were dramatically altered. Since new dimensions vary and are unknown the data analysis process will be complicated. For that reason, the specimen was not analyzed for this particular research.

After the concrete had been poured into the forms and cured for five days, the specimens were removed from their molds. Scanning was performed on the top face and the smooth side face of specimen 1. The scan function that was used was the grid scan. Grid scan mainly displays the distribution of grid distributed rebar through a grid diagram, location of rebar and thickness of cover and the same time [*]. This scanning method allows to select X axis and Y axis. When rebar is located the sensor beeps and a drawing of the rebar appears in the screen in the detected position. The hoops were test in the X-axis. For both top and side view ten tests that detected the correct number of rebar were done. When scanning for the rebar the Y-axis was used. The rebar was measured five times in between the length of every one feet. For X-axis the scan was done from left to right. On the other hand, for the Y-axis the direction of the scan was from down to up (Use Fig 1 as reference).

V. Results and Discussion

The experimental dimensions for a R/C beam/column like structure was studied using the ZBL-R630A rebar scanner in grid scanning mode. It was expected to read with the apparatus the detection, depth, distance, position and diameter of the rebar. However, the latter was not achieved during grid scan since the reading was not available. Furthermore, when performing General Scan if sensor is place directly above rebar diameter should be obtained by pressing the up key [3]. Even though, the general scan should detect diameter, it is not convenient for our sample since it has reinforcement in multiple directions. When using General Scan function axis cannot be selected and grid is not displayed on screen. Therefore, the sensor is more sensitive and can beep even if rebar is not parallel to it. In this case, when performing General Scan, the diameter was not detected for every rebar and in very many cases the results it yielded were outliers.

Table 1 shows the comparisons of the Depth of the rebar or C.C. between the values measured in the laboratory and the average values from the scanning test performed on the top side of the 17"x8"x8' column along the x-axis. Furthermore, Table 2 compares the values of the position of each rebar starting along the specimen starting at cero. Table 3, shows the distance between one ring to the next one. Tables 4, 5 and 6 show this same information but from when the specimen is tested on the smooth side face. The error percent for all the data was calculated using (1).

$$Error\ \% = \frac{|Experimental - Accepted|}{Accepted} \times 100\% \qquad (1)$$

TABLE 1 Depth Test for Steel Hoops on Top Face

Ring	Accepted Value (mm)	Experimental Average (mm)	Error Percent (%)
1	44.5	46.9	5.39
2	44.5	45	1.12
3	44.5	47.8	7.42
4	38.1	47.8	25.46
5	38.1	51	33.86
6	38.1	39.1	2.62
7	38.1	36	5.51
8	31.8	38.4	20.75
9	35.05	35.8	2.14
10	38.1	44.2	16.01
11	41.4	45.2	9.18
12	38.1	44.1	15.75
13	38.1	47.3	24.15
14	35.05	48.5	38.37
15	38.1	47.4	24.41

TABLE 2 Position Test for Steel Hoops on Top Face

Ring	Accepted Value (mm)	Experimental Average (mm)	Error Percent (%)
1	92.2	50.6	45.12
2	206.5	149.6	27.55
3	289.05	237.7	17.77
4	409.7	342.3	16.45
5	635.25	549.1	13.56
6	822.71	758.3	7.83
7	1013.21	967.3	4.53
8	1235.46	1150.2	6.90
9	1419.61	1366.6	3.73
10	1637.03	1561.8	4.60
11	1827.53	1755.2	3.96
12	2056.13	1982.6	3.58
13	2157.73	2090.7	3.11
14	2227.58	2190.1	1.68
15	2327.66	2291.7	1.54

TABLE 3 Separating Distance for Steel Hoops on Top Face

Ring	Accepted Value (mm)	Experimental Average (mm)	Error Percent (%)
1 to 2	114.3	99	13.39
2 to 3	82.55	88.1	6.72
3 to 4	120.65	104.6	13.30
4 to 5	225.55	206.8	8.31
5 to 6	187.45	209.2	11.60
6 to 7	190.5	209	9.71
7 to 8	222.25	182.9	17.71
8 to 9	184.15	216.4	17.51
9 to 10	217.42	195.2	10.22
10 to 11	190.5	193.4	1.52
11 to 12	228.6	227.4	0.52
12 to 13	101.6	108.1	6.40
13 to 14	69.85	99.4	42.30
14 to 15	100.08	101.6	1.52

TABLE 4 Depth Test for Steel Hoops on Side Face

Ring	Accepted Value (mm)	Experimental Average (mm)	Error Percent (%)
1	25.4	28.6	12.60
2	26.99	26	3.67
3	27.78	28.9	4.03
4	29.37	32	8.95
5	33.34	34.9	4.68
6	35.72	39.7	11.14
7	38.1	34.2	10.24
8	36.51	37.8	3.53
9	34.93	38	8.79
10	35.72	37.9	6.10
11	33.34	36.8	10.38
12	30.16	35.4	17.37
13	30.16	29.2	3.18
14	29.37	27.9	5.01
15	30.16	24	20.42

TABLE 5 Position Test for Steel Hoops on Side Face

Ring	Accepted Value (mm)	Experimental Average (mm)	Error Percent (%)
1	85.85	63.3	26.27
2	187.45	164.1	12.46
3	289.05	237.6	17.80
4	400.3	340.9	14.84
5	613.16	567	7.53
6	816.36	751.8	7.91
7	1013.21	994.4	1.86
8	1246.63	1176.8	5.60
9	1410.21	1394.4	1.12
10	1613.41	1587.9	1.58
11	1818.13	1776.9	2.27
12	2019.81	1987.3	1.61
13	2121.41	2104.6	0.79
14	2232.66	2183.7	2.19
15	2334.26	2297	1.60

TABLE 6 Separating Distance for Steel Hoops on Side Face

Ring	Accepted Value (mm)	Experimental Average (mm)	Error Percent (%)
1 to 2	114.3	99	13.39
2 to 3	82.55	88.1	6.72
3 to 4	120.65	104.6	13.30
4 to 5	225.55	206.8	8.31
5 to 6	187.45	209.2	11.60
6 to 7	190.5	209	9.71
7 to 8	222.25	182.9	17.71
8 to 9	184.15	216.4	17.51
9 to 10	217.42	195.2	10.22
10 to 11	190.5	193.4	1.52
11 to 12	228.6	227.4	0.52
12 to 13	101.6	108.1	6.40
13 to 14	69.85	99.4	42.30
14 to 15	100.08	101.6	1.52

Before starting the test, the position where the steel hoops were supposed to be was marked. The scanner was able to detect accurately were the hoops were at always at or very near to the mark. If the test was performed correctly the sensor detected the right amount of hoops. On occasions, it detected the same ring twice, however this can be avoided if the scanner is moved at a constant and reasonable velocity. The most troublesome reading is that of the first ring. If the ring is close to the starting point of reading the scanner can make the beeping noise detecting it, however it is possible that the drawing of this ferrous material does not appear in the grid diagram with its respective information.

Tables 7 through 9 describe the depth, position and distance of the two $^1/_2$" diameter rebar located in the top face. The scanning process for this side was more complicated due to the limited space to place and roll the sensor. These tests were done in the Y-axis direction. It was also performed with the option for dense rebar scanning on since the C.C. to the rebar in this scenario should be greater. Therefore, the rebar is harder to detect. In some cases, when performing these scans, the sensor had to be run over back and forth on top of the known position of the second rebar so it could be read by the scanner.

TABLE 7 Rebar Depth to Top Face

Distance (ft)	Accepted Value (mm)		Experimental Average (mm)		Error Percent (%)	
	Upper	Bottom	Upper	Bottom	Upper	Bottom
0-1	60.45	52.32	53.4	47	11.66	10.17
1-2	63.5	49.28	63.8	53	0.47	7.55
2-3	66.8	45.97	53	45.2	20.66	1.68
3-4	54.1	47.75	61.6	50.4	13.86	5.55
4-5	69.85	50.8	47.6	45.8	31.85	9.84
5-6	69.85	54.1	64.4	55.8	7.80	3.14
6-7	63.5	57.15	53	53.6	16.54	6.21
7-8	55.63	55.63	53	52.6	4.73	5.45

TABLE 8 Rebar Position Test on Top Face

Distance (ft)	Accepted Value (mm)		Experimental Average (mm)		Error Percent (%)	
	Upper	Bottom	Upper	Bottom	Upper	Bottom
0-1	60.45	52.32	103	18.6	70.39	64.45
1-2	63.5	49.28	17	54.4	73.23	10.39
2-3	66.8	45.97	88.2	19.6	32.04	57.36
3-4	54.1	47.75	89.6	26.2	65.62	45.13
4-5	69.85	50.8	91.2	27.6	30.57	45.67
5-6	69.85	54.1	73.8	16.6	5.65	69.32
6-7	63.5	57.15	91.2	27.6	43.62	51.71
7-8	55.63	55.63	93.2	41.8	67.54	24.86

TABLE 9 Rebar Separating Distance on Top Face

Distance (ft)	Accepted Value (mm)	Experimental Average (mm)	Error Percent (%)
0-1	84.4	79.38	6.32
1-2	88.8	79.38	11.87
2-3	68.6	82.55	16.90
3-4	63.4	85.73	26.05
4-5	63.4	88.9	28.68
5-6	57.2	93.66	38.93
6-7	63.6	88.9	28.46
7-8	51.4	85.85	40.13

Tables 10 through 12 summarize the information on depth, position and distance gathered from scanning tests performed on the side face of the beam/column. This scans were done in the Y-axis direction and using the dense rebar scanning method.

TABLE 10 Rebar Depth to Side Face

Distance (ft)	Accepted Value (mm)			Experimental Average			Error Percent (%)		
	Upper	Center	Bottom	Upper	Center	Bottom	Upper	Center	Bottom
0-1	47.63	42.86	44.45	37	32.8	36	22.32	23.47	19.01
1-2	44.45	44.45	46.04	51	46.4	51.2	14.74	4.39	11.21
2-3	55.56	47.63	46.04	52.6	48.8	49	5.33	2.46	6.43
3-4	55.56	49.21	47.63	52.2	47.8	48.2	6.05	2.87	1.20
4-5	55.56	47.63	44.45	50.2	44.8	43.8	9.65	5.94	1.46
5-6	41.28	44.5	41.28	49.2	46.8	43.8	19.19	5.17	6.10
6-7	44.45	38.1	36.51	45	43	40.4	1.24	12.86	10.65
7-8	41.4	31.75	39.62	43	33.2	35	3.86	4.57	11.66

TABLE 11 Rebar Position Test on Side Face

Distance (ft)	Accepted Value (mm)			Experimental Average (mm)			Error Percent (%)		
	Upper	Center	Bottom	Upper	Center	Bottom	Upper	Center	Bottom
0-1	379.48	215.9	44.45	323.2	176	25.6	14.83	18.48	42.41
1-2	382.52	215.9	46.04	335	177.6	28.8	12.42	17.74	37.45
2-3	382.52	215.9	46.04	332	175.8	25.6	13.21	18.57	44.40
3-4	385.83	215.9	47.63	339.4	182.8	29	12.03	15.33	39.11
4-5	381	212.73	44.45	325.6	172.8	19.8	14.54	18.77	55.46
5-6	377.95	212.73	41.28	329.4	178.6	19	12.85	16.04	53.97
6-7	374.65	212.73	36.51	328.4	172.2	19	12.34	19.05	47.96
7-8	376.17	215.9	39.62	322	178	23.4	14.40	17.55	40.94

TABLE 12 Rebar Separating Distance on side Face

Distance (ft)	Accepted Value (mm)		Experimental Average (mm)		Error Percent (%)	
	Bottom-Center	Center-Upper	Bottom-Center	Center-Upper	Bottom-Center	Center-Upper
0-1	153.99	165.1	156.2	158.6	1.44	3.94
1-2	157.16	163.51	157.8	151.6	0.41	7.28
2-3	146.05	163.51	152.2	150.8	4.21	7.77
3-4	149.23	158.75	155.4	148.4	4.13	6.52
4-5	149.23	161.93	154.4	151.6	3.46	6.38
5-6	163.51	165.1	148.8	153.8	9.00	6.84
6-7	160.34	169.86	147.2	153.0	8.20	9.93
7-8	165.1	160.27	151.6	153.8	8.18	4.04

VI. Future Works

There is much that can be improved and is yet to be done for this research. For starters, gathering more data from the other two sides of specimen 1 and compare them. Also, test different structures e.g. specimen 2 (12”x12”x8’) which is already built and a wall/floor like structure. A very important feature of reinforcement is its size (diameter). Therefore, it is important to work with the scanner so that the diameter can be read when performing tests.

Furthermore, the future scope of this work is to test it on the field in creole hillside construction to analyse what type of rebar is commonly used. This information can be significant to studying effects of earthquake loads in these structures.

Conclusions

The ZBL-R630A rebar scanner was used to perform grid scans on a 17”x8”x8’ column representative structure. The measures were taken on two sides of the structure (top face and side face). Both side were scanned individually for in the x-axis for steel hoops and y-axis for rebar. The information obtained from the scans were first the detection of the ferrous material and then depth (C.C.), position and distance. As per detection, if using Grid Scan function and testing parallel to rebar, the scanner is reliable. However, this does not mean that the position of the detected ferrous structure will be accurate. Even though it can be accurate, it can be affected by were the user begins the test, the speed of test and reverse movement. Position was the dimension with higher error for the rebar in both faces. For the steel hoops the position was more erroneous for the first hoops in the beginning of the scan and closest to the accepted values as it kept going further in the length of the column. On the other hand, for the steel hoops in top view and side view they had an average error percent of 15.48% and 8.67% respectively. Also, the distance between hoops had an average error percent of 11.48% for the top view perspective and 13.72% to the side face. It must be noted that readings regarding the hoops could’ve varied for each test because of the non-uniform shape of the hoops.

For the rebar scanned from the top, the bottom rebar had an average error percent in depth of 6.20% and the upper rebar of 13.45%. Furthermore, the average error for the distance in between the two rebar was 24.67%. From the side view perspective, the average error percents for depth were 8.47%, 7.71% and 10.30% from bottom to upper rebar. The distance from the bottom rebar to the center rebar resulted in an average error of 1.46%, while from center to upper rebar yielded 6.59%.

When performing a grid scan, the ZBL-R630A is and useful tool to detect rebar and obtain information that gives an idea or diagram of how the reinforcement is distributed throughout the structure, however it is not highly precise and results can vary from test to test.

Acknowledgments

I would like to thank Rolando García for his mentorship and guidance. Also, my gratitude to all the students and faculty members that offered their help when it was much needed and made the construction of the beams possible.

References

[1] American Concrete Institute (ACI-318-11) (2011) “Building Code Requirements for Structural Concrete”, American Concrete Institute.

[2] Beijing ZBL Science & Technology Co., Ltd. (N.D.). Operation Manual..

[3] González, Y. (2015). Rehabilitation of RC Residential Houses on Gravity Columns Over Slope Terrain. Ph.D. Thesis, University of Puerto Rico, Mayaguez Campus.

[4] Vázquez, D. (2002). “Seismic Behavior and Retrofitting of Hillside and Hilly Terrain of R/C Houses on Gravity Columns.”, Ph.D. Thesis, Department of Civil Engineering, University of Puerto Rico, Mayagüez Campus.

Clean Technologies Research

Mentors

Amaury Malavé, PhD
School of Engineering
Universidad del Turabo, Gurabo, PR, USA

Frank Valentín, MD
School of Health Science
Universidad del Turabo, Gurabo, PR, USA

Ileana González, PhD
School of Natural Science and Technology
Universidad del Turabo, Gurabo, PR, USA

José R. Pérez, PhD
School of Natural Science and Technology
Universidad del Turabo, Gurabo, PR, USA

Lisandro Cunci, PhD
School of Natural Science and Technology
Universidad del Turabo, Gurabo, PR, USA

Rolando García, PhD
School of Engineering
Universidad del Turabo, Gurabo, PR, USA

Wilma Pabón, MSE
School of Engineering
Universidad del Turabo, Gurabo, PR, USA

Karleen González, MS student
School of Natural Science and Technology
Universidad del Turabo, Gurabo, PR, USA

Jayleen Díaz, MS student
School of Natural Science and Technology
Universidad del Turabo, Gurabo, PR, USA

Dayna Ortíz, MS student
School of Natural Science and Technology
Universidad del Turabo, Gurabo, PR, USA

Luis López, MS student
School of Natural Science and Technology
Universidad del Turabo, Gurabo, PR, USA

Authors

Authors

Clean Technologies Research

Students

Jorge Santiago
Chemistry Student at Universidad del Turabo, Gurabo, PR, USA

Kemuel Torres
Electrical Engineering Student, at Universidad del Turabo, Gurabo, PR, USA

Paola Carrión
Biology Student at Universidad del Turabo, Gurbao, PR, USA

Pedro J. Guisti
Computer Engineering at Universidad del Turabo, Gurabo, PR, USA

Jeffrey R. Cruz
Computer Engineering at Universidad del Turabo, Gurabo, PR, USA

Lichel Báez
Biology Student at Universidad del Turabo, Barceloneta, PR, USA

John González
Chemistry Student at Universidad del Turabo, Gurabo, PR, USA

Eimilyn Achahg
Mechanical Engineering at Universidad del Turabo, Gurabo, PR, USA

Angel Mangual
Mechanical Engineering at Universidad del Turabo, Gurabo, PR, USA

Stephanie Alsina
Chemistry Student at Universidad del Turabo, Gurabo, PR, USA

Frankie Rolón
Chemistry Student at Universidad del Turabo, Gurabo, PR, USA

Tiara Polanco
Chemistry Student at Universidad del Turabo, Gurabo, PR, USA

Ariana Del Mar Irizarry
Biology Student at Universidad Metropolitana, San Juan, PR, USA

Alejandra López
Civil Engineering at Universidad del Turabo, Gurabo, PR, USA

Tiffany Del Valle
Biology Student at Universidad del Turabo, Gurabo, PR, USA

Solimar Garcia
Biology Student at Universidad del Turabo, Gurabo, PR, USA

Jonathan López
Biology Student at Universidad del Turabo, Gurabo, PR, USA

Christian Del Valle
Biology Student at Universidad del Turabo, Gurabo, PR, USA

Authors

Authors

Clean Technologies Research

Armando Soto Guerrero, BA
Web Master at Universidad del Turabo,
Gurabo, PR, USA

Darlene Muñoz Villafañe, BA
Administrative Director of Research Project at
Puerto Rico Energy Center & ACT Global, Gurabo,
PR, USA

Ián Gutiérrez Molina, Eng.
Lab Technitan at
Puerto Rico Energy Center (PREC),
Gurabo, PR, USA

Josefina Melgar, MS
Compliance Coordinator by
Vicechancellor's Office Affairs at
Universidad del Turabo, Gurabo, PR, USA

Sandra R. Pedraza Torres, MSE
Innovation and Commercialization Director by
vicechancellor's Office Afairs at
Universidad del Turabo, Gurabo, PR, USA

Suheilie Rodríguez González, BS
Editor of Summer Internship Proceeding's at
Universidad del Turabo, Gurabo, PR, USA

Sandra Mendez Pagán
Administrative Asistant of Puerto Rico Energy Center,
(PREC), Gurabo, PR, USA

Amaury Malavé Sanabria, PhD
Executive Director of Puerto Rico Energy Center
(PREC), Gurabo, PR, USA

Jannette Pérez, MSE
Professor at School of Engineering at
Universidad del Turabo, Gurabo, PR, USA

Pedro Anibarro
Student at School of Engineering at
Universidad del Turabo, Gurabo, PR, USA

Collaborators

Collaborators

TURABO | UNIVERSIDAD DEL TURABO
SISTEMA UNIVERSITARIO ANA G. MÉNDEZ